DIFFERENTIATED INTRA- AND INTER-AGGREGATE WATER CONTENT MODELS OF MX-80 BENTONITE

Authors' postprint version of the paper published in *Applied Clay Science*:

Navarro V, Asensio L, De la Morena G, Pintado X and Yustres Á (2015) Differentiated intra- and inter-aggregate water content models of MX-80 bentonite. Applied Clay Science 118:325-336.

doi: 10.1016/j.clay.2015.10.015

DIFFERENTIATED INTRA- AND INTER-AGGREGATE WATER CONTENT MODELS OF MX-80 BENTONITE

Vicente Navarro [*a], Laura Asensio [a], Gema De la Morena [a], Xavier Pintado [b] and Ángel Yustres [a]

[a] Geoenvironmental Group, Civil Engineering Department, University of Castilla-La Mancha, Avda. Camilo José Cela s/n, 13071 Ciudad Real, Spain

[b] B+Tech Oy, Laulukuja 4, 00420 Helsinki, Finland

[*]Corresponding author. Email address: vicente.navarro@uclm.es; Tel. +34 926295300 ext. 3264; Fax +34 926295391

ABSTRACT

The current research proposes a method for obtaining the intra-aggregate (microstructural) and inter-aggregate (macrostructural) water content of MX-80 bentonite using data from water retention curves. Data associated with high suction were used to define the microstructural water content model. By extrapolating this model to low suction, microstructural and macrostructural water contents were separated to obtain a macrostructural water content model. Micro- and macrostructural water content models have been used to simulate an isotropic swelling test, thus illustrating the advisability of using a double and differentiated macro/micro description of the water content to characterise the hydro-mechanical behaviour of MX-80 bentonite.

KEYWORDS

Bentonite; double porosity; water content; disaggregated model; microstructure

1. INTRODUCTION

According to experimental observations by various authors who have studied the fabric of compacted expansive clays, the pore-size distribution function of these materials generally displays a distinct bimodal character (see Delage *et al*., 1996, Romero *et al.*, 1999, Lloret *et al*., 2003, Delage *et al*., 2006, Romero *et al*. 2011 and references therein). As established by Gens and Alonso (1992), Alonso *et al*. (1999), Sánchez *et al*. (2005), Musso *et al*. (2013) and Guimarães *et al*. (2013), among others, it is advisable to use double porosity models when simulating the thermo-hydro-chemo-mechanical behaviour of these materials. In these works, two structural levels are considered: the macrostructural level, which is composed of global arrangements of clay aggregates with pores between them (Sánchez *et al*., 2005), and the microstructural level, which corresponds to the intra-aggregate porosity. Gerke and van Genuchten (1993a, b) proposed a similar model to analyse the flow of water and solutes in a structured soil. In principle, the water located within the pores between aggregates (macrostructural water) might have a chemical potential that differs from that of the water stored inside the aggregates (microstructural water). In such a case, a diffusion-type process of mass exchange (Guimarães *et al*., 2013) will occur that might not be instantaneous and could play an important role in the time-dependent deformation of soils (see Wilson and Aifantis, 1982; Ghafouri and Lewis, 1996; Alonso *et al*., 1991; Gens *et al*. 2011). These transient processes also occur when water retention curves (WRCs) are characterised (Dueck, 2008). However, the water content is usually measured after the transient processes are finished and equilibrium in suction is reached (Delage, 2002).

Still, even under equilibrium conditions, it is advisable to differentiate between the microstructural and macrostructural water content when simulating bentonite behaviour (Alonso *et al*., 2011; Gens *et al*., 2011). In this way, it is possible to determine the

macrostructural void ratio and degree of saturation. The macrostructural void ratio constrains the macrostructural intrinsic permeability, and the macrostructural degree of saturation is required to obtain the macrostructural relative permeability. Relative and intrinsic permeabilities define the macrostructural advective flow, which is instrumental for correctly formulating the water mass balance. Thus, it is worthwhile to define differentiated hydraulic models of the microstructural and macrostructural water content.

The following sections discuss a procedure to obtain these models from WRCs. First, experimental data obtained for high suction values (greater than 20 MPa) are used to model the microstructural water content and void ratio. Second, this microstructural model is extrapolated for suctions of less than 20 MPa to differentiate the microstructural and macrostructural water content. The results obtained in this manner are used to define the macrostructural water content model. Finally, the parameters deduced from the application of the model to the WRCs results were used to simulate an isotropic swelling test illustrating the scope and limitations of the proposed models.

2. MATERIALS, METHODS AND EXPERIMENTAL DATA

The WRCs of different batches of MX-80 bentonite were analysed in this work. First, a Volclay MX-80 material whose physical properties correspond to those obtained by Kumpulainen and Kiviranta (2010) (see Table 1) was tested in B+Tech's laboratory. The isothermal (25º C) paths in compacted samples under constant volume shown in Table 2 were used to determine the WRCs in an adapted oedometric cell. The vapour equilibrium technique was used to control suction during the tests. In this technique, control of the relative humidity (*RH*) of the air surrounding the specimen allows

imposition of a total suction (s) because both magnitudes are related by the equation (Edlefsen and Anderson, 1943):

$$s = \frac{R \cdot T \cdot \rho_w}{M_w} \mathrm{Ln}\,(RH) \quad [1]$$

where R is the universal gas constant, T is the absolute temperature, ρ_w is the water density and M_w is the molar mass of water. Relative humidity is usually applied by varying the salinity of an aqueous solution (see, among others, Yahia-Aïssa, 1999; Dueck, 2004; Delage *et al.*, 2008; Pintado *et al.*, 2009). With this procedure, it is possible to obtain suction values of up to 1000 MPa (Pintado *et al.*, 2009).

Samples of 35 mm in diameter and approximately 16 mm high with different initial dry densities (from some 1400 kg/m^3 to almost 1700 kg/m^3) and water content values (between 4.6% and 6.2% hygroscopic water content under laboratory conditions) were tested (see Table 2). The total suction s_f was imposed in only one step by pumping relative-humidity-controlled air through an upper porous stone. The bottom porous stone was a no-flow boundary. The sample was assumed to reach a total suction that was close to the imposed suction when the swelling pressure reading (measured with a load cell installed on top of the sample) became stable. Moreover, the steady-state conditions were verified by measuring the *RH* at the top and bottom of the sample using a capacitive hygrometer. A special piston and bottom plate were used to secure the hygrometer probes. After equilibrium was reached, the samples were extracted from the cell and the water content w_f (Table 2) was determined using the ASTM standard test method D2216-10 (ASTM, 2010). The values of s_f were measured using a chilled-mirror dew-point psychrometer (Gee *et al.*, 1992; Leong *et al.*, 2003). The obtained results are presented in Fig. 1.

In addition, the results from Dueck and Nilsson (2010) plotted in Fig. 2 were also analysed. The properties of the material used ("Wym") are listed in Table 1 (values

adopted from Karnland *et al*., 2006). These tests were conducted at 20ºC under free swelling conditions. In all cases, the vapour equilibrium technique was used to impose the total suction. Figure 2 also includes results from Wadsö *et al*. (2004) and Kahr *et al*. (1990) that were obtained in tests similar to those conducted by Dueck and Nilsson (2010). The total suction (s) values shown in Fig. 2 were obtained using Eq. 1.

Finally, with respect to experimental work, an isotropic swelling test was performed in the laboratory at the University of Castilla-La Mancha. A cylindrical sample of the same MX-80 bentonite employed in the tests in Fig. 1 was uniaxially compacted. The sample that had a diameter of 50 mm and an initial height of 25 mm. It had an initial bulk density of 2.03 g/cm^3 and an initial water content of 20%. Using these values, and assuming the grain density of Table 1, the initial dry density ρ_d, total void ratio e (total volume of voids per volume of mineral) and degree of saturation S_r were computed, as indicated in Table 3.

The test run for 65 days under isothermal conditions (22ºC). The sample was subjected to a constant cell pressure of 1.1 MPa in a triaxial apparatus with no contact between the top of the sample and the cell piston. Therefore, the test was performed under spherical stress conditions. A porous stone in contact with atmospheric conditions was placed on top of the sample. Free hydration with de-ionised water at atmospheric pressure was allowed at the bottom of the sample.

An automated system with two pressure/volume controllers was used for the test; one controller was used for the cell pressure and the other was connected to the bottom of the sample for the water injection pressure. No local strain transducers were used. The volume change data from the volume gauge in the cell controller were used to compute the volumetric strain ε_V. The cell deformation and the lab temperature variation were took into consideration to identify the volumetric strain trend of the soil. To this end, a

detrending approach usually used when non-stationary time series are analysed was applied to filter ε_V from the raw data (Salas et al., 1980). Although uniaxially compacted samples tend to swell more in the axial direction, as the sample was held under isotropic conditions, the axial strain ε_Z was assumed to be ε_V /3. The vertical swelling values plotted in Fig. 3 were derived using this procedure.

3. MODEL DEVELOPMENT

To separate the microstructural water content values from the total water content values shown in Figs. 1 and 2, the total soil water content was assumed as the sum of the water that partially fills the inter-aggregate voids ("macrostructural" water) and the water stored inside the intra-aggregate porosity ("microstructural" water) (see Alonso *et al*., 2011; Della Vecchia *et al*., 2012; and Casini *et al*., 2012, among others). According to Or and Tuller (1999) and Tuller and Or (2005), it was accepted that capillary contributions from the water held in the macropores dominated in the wetter range of the WRC. In addition, the adsorptive contributions were considered dominant in the dryer range of the curve, with the soil water content primarily occurring in the micropores. The results obtained by Or and Tuller (1999) indicate that the capillary contributions become negligible for a wide range of soil textures for suction values greater than 10 MPa. Romero *et al*. (2011) identified the suction corresponding to empty macropores and fully saturated micropores as 25 MPa for FEBEX bentonite (for a complete description of this material, see Enresa, 2000). Jacinto *et al*. (2009) found that, for MX-80 bentonite, the dry density influences the water retention capacity for suction less than approximately 30 MPa, which would be the lower limit for a region dominated by adsorptive storage mechanisms (Romero *et al*., 2011). In the current work, it has been assumed that the water content values from Figs. 1 and 2 are

fundamentally associated with intra-aggregate water for suction values higher than 20 MPa.

Starting from a notably dry condition, the initial stages of hydration are associated with crystalline swelling. Several authors have contributed valuable descriptions of this process (Barshad, 1955; Pusch, 1983; Kahr *et al*., 1990; Laird, 1996; and Salles *et al*., 2009), which is characterised in Fig. 4, adapted from Cases *et al*. (1992). Two possible functional structures were considered for the description of this behaviour. First, the application of the potential law proposed by Tuller and Or (2005) was analysed:

[2] $$w_{mC} = \sqrt[3]{\frac{A}{6\pi s_m}}\, S \cdot \rho_{Wm}$$

where w_{mC} is the crystalline microstructural water content in percentage, A is the modulus of the Hamaker constant ($6 \cdot 10^{-20}$ J; Tuller and Or, 2005), s_m is the microstructural suction, S is the clay specific surface area (in units of m^2/kg) and the microstructural water density ρ_{wm} is expressed in kg/m^3. Several works have shown that the density of adsorbed water is greater than that of free water ρ_W (see, e.g., the review in Hueckel, 1992). More recently, Jacinto *et al*. (2012) analysed the influence of water density on the water retention properties of expansive clays. According to their work, the density of adsorbed water in MX-80 bentonite at a suction of 100 MPa is close to 1.17 g/cm^3. However, if instead of that density, the density of free water (ρ_W = 1 g/cm^3) is taken in the calculations, the volume of microstructural water could then be overestimated by 17 %. For this reason, it is advisable to study the sensitivity of the models to the value of ρ_{Wm}. The evolution of water density with suction proposed by Jacinto *et al*. (2012) can be used for this purpose. In such an exercise, it was verified that the error derived from assuming ρ_{Wm} equals ρ_W does not substantially affect the outcome of the calculations in the current work, and differences of less than 15% were

obtained. Therefore, the free and adsorbed water densities were assumed to be equal for modelling purposes (as in Tournassat and Appelo, 2011).

De-ionised water was used to prepare the samples of the tests in Figs. 1 and 2 (Dueck and Nilsson, 2010; Pintado *et al*., 2013), and the samples were subsequently hydrated by adding pure water from vapour condensation. This fact does not imply that osmotic suction can be disregarded. The original osmotic suction given by the chemical composition of the material independently of the salinity of the water added does not necessarily have to be zero. Although this original value can be reduced when de-ionised water is added, in many of the analysed cases the samples did not reach a high degree of saturation, and no significant dilution took part. Therefore, the original osmotic suction remained almost constant. However, in bentonite clays the structural component (in the sense of Low, 1987) of suction is so high that the osmotic component can be neglected. Hence, the microstructural suction (given in Pa units in Eq. 2) at equilibrium with the macrostructural water can be calculated as (Navarro *et al*., 2013):

$$s_m = p + s_M \quad [3]$$

where s_M is the macrostructural matric suction ($s_M = P_G - P_L$, where P_G is the gas pressure and P_L is the pressure of macrostructural liquid) and p is the net mean stress ($p = p_{TOT} - P_G$, where p_{TOT} is the mean stress).

In addition to the potential law of Tuller and Or (2005), the application of a van Genuchten (1980) type curve (VG) was also considered to model w_{mC}. This curve was proposed by Durner (1994) to describe the retention characteristics of soils with heterogeneous pore systems and was adopted by Gerke and van Genuchten (1993a) for dual-porosity soils and Della Vecchia *et al*. (2014) for compacted clays. Similarly, a VG model was employed to describe the microstructural degree of saturation in an analysis

of clay soils by Alonso *et al*. (2011) and in a study of compacted silts by Casini *et al*. (2012).

Cases *et al*. (1992) indicated that crystalline swelling is practically complete when the suction reaches approximately 44 MPa (*RH* of 72% at 20ºC). For lower suctions, the hydration dynamics change, and the processes known as "osmotic swelling" (or "double layer swelling"; Laird, 1996) become more relevant. To model the increase in microstructural water caused by this new wetting trend, the logarithmic law "Δw_{mO}", which is similar to that used by Dueck and Börgesson (2007), was adopted:

[4] $$\Delta w_{mO} = -B \cdot \mathrm{Ln}\left(\frac{s_m + P_{ATM}}{s_{mO} + P_{ATM}} \right)$$

where B is a material parameter and s_{mO} is the microstructural suction at which osmotic swelling begins to play a significant role (a value of 40 MPa has been assumed). Thus, the microstructural water content was calculated as follows:

[5] $$w_m = w_{mC} + \Delta w_{mO}$$

If one assumes that the increase in microstructural void space from the dry state is equal to the increase in microstructural water, then the following relationship holds:

[6] $$e_m = G_S \cdot w_m$$

where $G_S = \rho_S / \rho_W$ is the specific gravity of the soil particles, ρ_S is the density of mineral particles (see Table 1) and e_m is the microstructural void ratio (volume of voids in the microstructure per volume of clay mineral). Therefore, the definition of the microstructural water content directly implies the definition of a model of microstructural porosity and *vice versa*. Eq. 5 can be written as follows in terms of the microstructural void ratio:

[7] $$e_m = e_{mC} + \Delta e_{mO}$$

The VG model and Eqs. 2 and 4 can also be written using e_m. In particular, if the latter equation is written as a function of e_m, the following equation is obtained for s_m less than 40 MPa:

[8] $$\Delta e_{m0} = -\kappa_m \cdot \mathrm{Ln}\left(\frac{s_m + P_{ATM}}{s_{m0} + P_{ATM}}\right)$$

This expression, where κ_m is a microstructural stiffness parameter, was utilised by Sánchez *et al*. (2005), Alonso and Navarro (2005), Alonso *et al*. (2011) and Gens *et al*. (2011) to define the volumetric behaviour of the microstructure.

Once the model for the microstructural water content was defined, it was used to estimate w_m for suctions less than 20 MPa. The obtained values allowed to derive the macrostructural water content (w_M) by subtracting the estimated w_m values from the experimental water content (w) values: w_M=w-w_m (see Della Vecchia *et al*., 2012, for example). The w_M values obtained in this manner were used to define a model of the macrostructural retention law. A VG model was also applied, and s was used as a state variable.

A double porosity model (Gens and Alonso, 1992; Alonso *et al*., 1999; Sánchez *et al*., 2005; Guimarães *et al*., 2013) was adopted to simulate the swelling test in Fig. 3. In the simulation, equilibrium between macrostructural and microstructural water was not assumed: the water potentials in the two structural levels might be different, which leads to an exchange of water between them (Gens *et al*., 2011). Therefore, a mass exchange term c_m between the two levels was included when analysing the mass balance of both micro and macrostructural water. Hence, the macrostructural water mass balance was formulated as (Navarro *et al*., 2008):

[9] $$\frac{\partial m_M}{\partial t} + \nabla \cdot \left(m_M \cdot \mathbf{q}_M\right) + c_m = 0$$

where $m_M = (\rho_W \cdot S_{rM} \cdot e_M) / (1+e)$ is the mass of macrostructural water per unit volume, S_{rM} is the macrostructural degree of saturation, e_M is the macrostructural void ratio, $\mathbf{q}_M$ is the macrostructural water seepage, $\partial/\partial t$ is the time derivative and $\nabla\cdot$ is the divergence operator. Although other authors have proposed first-order water transfer models (Gerke and van Genuchten, 1993a, b; Musso *et al*., 2013), a non-linear formulation was adopted to define c_m (Navarro *et al*., 2013):

$$\frac{c_m}{\rho_W} = H \cdot \left(\frac{p + s_M}{s_m} \right)^C \cdot \left(s_m - \left(p + s_M \right) \right) \quad [10]$$

where the parameter H defines the transfer coefficient at the end of the mass exchange process (when $s_m = s_M + p$) and parameter C describes the mass transfer change as s_m approaches s_M. Consistent with the results obtained by Navarro *et al*. (2013) after analysing an MX-80 bentonite test by Montes-H *et al*. (2003), the values $H=1.5\cdot10^{-8}$ $(kPa\cdot s)^{-1}$ and $C=0.4$ were assumed.

The macrostructural water seepage $\mathbf{q}_M$ vector was calculated as follows:

$$\mathbf{q}_M = -\frac{k_{rM} \cdot k_{iM}}{\mu_W} \cdot \left(\nabla P_L + \rho_W \cdot g \cdot \nabla z \right) \quad [11]$$

where k_{rM} is the relative permeability, k_{iM} is the isotropic intrinsic permeability, μ_W is the dynamic viscosity of water, g is the gravity constant and z is the vertical coordinate. The Brooks and Corey (1964) and Burdine (1953) formulation with an exponent value equal to 3 (Börgesson and Hernelind, 1999; Gens *et al*., 2011) was used to model the relative permeability as a function of the macrostructural degree of saturation:

$$k_{rM} = \left(S_{rM} \right)^3 \quad [12]$$

An intrinsic permeability expressed as a function of the macrostructural porosity ϕ_M $=e_M / (1+e)$ was adopted (Gens *et al*., 2011):

$$k_{iM} = k_{MO} \cdot \exp\left(b\left(\phi_M - \phi_{MO} \right) \right) \quad [13]$$

where b is a material parameter and ϕ_{MO} is a reference macrostructural porosity for which the intrinsic permeability is k_{MO}. Using the data from Karnland *et al*. (2006), the parameters $k_{MO}=9.94\cdot10^{-21}$ m^2, $b=9.18$ and $\phi_{MO}=0.053$ were identified.

The microstructural water mass balance equation was formulated as follows:

$$\frac{\partial m_m}{\partial t} - c_m = 0 \quad [14]$$

where $m_m=(\rho_W\cdot e_m)/(1+e)$ is the mass of microstructural water per unit volume. Similar to the immobile water of van Genuchten and Wierenga (1976), the microstructural water was considered linked to the soil skeleton.

The above formulation was implemented in the multiphysics partial differential equations solver COMSOL Multiphysics (Comsol AB, 2011) to simulate the isotropic swelling test. The numerical strategies described by Navarro *et al*. (2014b) were applied. The solution of Eqs. 9 and 14 allows calculation of the state variables P_L and e_m.

4. DETERMINATION OF MODEL PARAMETERS FROM WRCs RESULTS

To analyse the validity of Eq. 2, the product $w_m\cdot s_m^{1/3}$ is represented in Fig. 5a, as obtained with data from the tests of Fig. 2. Only data from suctions greater than 40 MPa ($w = w_m = w_{mC}$) were used. As shown, the relationship is not constant. According to Eq. 2 and as highlighted by Cases *et al*. (1992) and Salles *et al*. (2009), among others, this result appears to indicate that the clay specific surface area is not constant throughout the hydration process. Therefore, the data for s_m and w_m that were used in Fig. 5a are compared in Fig. 5b with the model of w_m that results from introducing into Eq. 2 the variation of S obtained by Salles *et al*. (2009) in their hydration analysis of a Na-montmorillonite (see Fig. 5c). The fit is not satisfactory.

Indeed, there is no reason to expect that the variation of S from the analysis of Na-montmorillonite in Salles *et al*. (2009) should exactly reproduce the variations of specific surface area in the MX-80 bentonite studied in this work. If all of the values of w_m and s_m from the tests of Fig. 2 are used, the value of S linked to each w_m - s_m point can be found through Eq. 2, obtaining the results in Fig. 5c. The identified law is different from that obtained by Salles *et al*. (2009). For suction values less than 40 MPa, the specific surface area begins to show a greater dispersion, which appears to confirm that a change in the hydration trend is produced near this value.

If reliable information on the evolution of S is not available beforehand, then application of Eq. 2 to obtain w_{mC} is not a simple task. Therefore, use of the VG model was considered because its sigmoidal shape can approximate the characteristic curve shown in Fig. 4. According to Eq. 6, the VG model was formulated in terms of the microstructural void ratio as follows:

[15] $$e_{mC} = \frac{e_{mCMAX}}{\left(1+\left(\alpha_m \cdot s_m\right)^{n_m}\right)^{l_m}}$$

where e_{mCMAX} is the microstructural void ratio associated with the crystalline swelling at saturation, and α_m and l_m are fitting parameters. The relationship n_m=1/(1-l_m) (van Genuchten, 1980) was assumed to be valid. Using experimental values from Fig. 2 associated with suctions greater than 40 MPa, values of e_m (identified with e_{mC}) were derived with Eq. 6, and a least-squares method was applied to obtain the parameters of Eq. 15 included in Table 4. Using these parameters, the fitting represented in Fig. 6 was obtained, which satisfactorily reproduces the aimed suction range (s_m>40MPa).

As illustrated in Fig. 7, the same is not true when tests 3_10_20 and 5_64_10, also performed by Dueck and Nilsson (2010) under free swelling conditions using the vapour equilibrium technique, are modelled ("emC" curve). These tests are different

from the 1_0_20 test because their initial bentonite water content was greater than zero (10% in 3_10_20 and 64% in 5_64_10). An offset occurrs between the model and the experimental values as if an "additional" microstructural void ratio (or microstructural water content) were present, which is not accounted for in Eq. 15. Thus, as observed in Fig. 4, a residual water content of 1.8% is identified for the Na-montmorillonite analysed by Cases *et al*. (1992) under dry conditions. According to Eq. 6, this result implies a microstructural void ratio e_{mR} of 0.048. If this value is introduced into the law for e_{mC} as follows:

[16] $$e_{mC} = e_{mR} + \frac{e_{mCMAX}}{\left(1+\left(\alpha_m \cdot s_m\right)^{n_m}\right)^{m_m}}$$

the fit to the experimental data improves (Fig. 7, "emC+emR(=0.048)" curve). This improvement is even more noticeable if an identification problem is solved for the value of e_{mR} that provides a better fitting to the experimental data (Fig. 7, "emC+emR_opt" curve). An "optimal" value for e_{mR} of 0.093 was obtained (Table 4). Again, only experimental data from Fig. 2 associated with suctions greater than 40 MPa were used to solve the identification problem.

Taking e_{mR} =0, the e_m data from the tests in Fig. 2 were used once again to identify the optimal value of the microstructural stiffness parameter κ_m. However, in this case, experimental values corresponding to the range between 20 MPa and 40 MPa were used, and the satisfactory fit shown in Fig. 8 was obtained for κ_m = 0.04 (Table 4). However, the quality of this fit has a limited scope because it is a consequence of the solution to several parameter identification problems.

Conversely, the fit presented in Fig. 9 is more remarkable. In this figure, the model of e_m obtained from the parameters presented in Table 4 is compared with the experimental results of Fig. 1. Because the parameters are based on the data of Fig. 2, they are

independent of the experimental results of Fig. 1. For this reason, the obtained fit is especially valuable and supports the microstructural model defined by the parameters of Table 4 and Eqs. 7, 8 and 16. Acceptance of this model for both the free swelling tests in Fig. 2 and the constant volume tests in Fig. 1 implies assumption of a one-to-one relationship between s_m and e_m independent of the applied macroscopic strain constraints, as certain authors have observed (see, among others, Villar, 2007; Romero *et al.*, 2011; Jacinto *et al.*, 2012).

When s_m approaches zero, the modelled e_m moves gradually towards the value of 0.8 (Fig. 9). This value is slightly lower than 0.9, the value identified by Pusch *et al*., (1990) and Bourg *et al*., (2006) for Na-bentonites and also by Romero *et al*. (2011) for an MX-80 bentonite. Nevertheless, this value is within the range that would result from assuming that the adsorbed water has an equivalent thickness of two or three water monolayers (see, among others, Sposito and Prost, 1982, and Cases *et al*., 1992) in a situation of destructuration of bentonite aggregates into nearly individual sheets (Neretnieks *et al*., 2009). In this case, e_m can be estimated with the ratio t/t_S. If the sheet thickness t_S is given a value of 1 nm, and the thickness of each water layer t is taken as 0.3 nm, the obtained microstructural void ratio values are between 0.6 and 0.9. For this reason, it was admitted as a working hypothesis that the extrapolation of the model of e_m defined by Eqs. 7, 8 and 16 and the parameters in Table 4 is valid for estimation of e_m for suctions less than 20 MPa.

After estimating e_m, w_m was computed, and the macrostructural water content w_M was derived by subtracting w_m from the total water content experimental values. In addition, using the values of the final dry density ρ_d shown in Table 2, the values of the total void ratio e were obtained, and using the estimated value of e_m, the value of the macrostructural void ratio e_M (volume of voids in the macrostructure per volume of

mineral, $e = e_M + e_m$) was deducted. In this manner, the wetting experimental values of the macrostructural degree of saturation S_{rM} presented in Fig. 10 ("SrM test data") were calculated. The same figure shows the values of the "total" degree of saturation S_r, which were obtained from w and ρ_d by assigning a unique characteristic curve to the soil without differentiating between the macrostructural and microstructural water. As expected, if there is no distinction between w_M and w_m, the S_r values are greater than S_{rM}. The experimental results of Villar (2007) on the main wetting path are also included in Fig. 10 for comparison purposes.

A VG model was fitted for both S_{rM} and S_r, according to the following laws:

[17] $$S_{rM} = \left[1 + \left(\frac{s}{P_M}\right)^{\frac{1}{1-l_M}}\right]^{-l_M}$$

[18] $$S_r = \left[1 + \left(\frac{s}{P}\right)^{\frac{1}{1-l}}\right]^{-l}$$

where P_M is the macrostructural air-entry pressure value. Parameters P_M, l_M, P and l were identified using a least-squares fitting procedure and the values indicated in Table 5 were obtained. The relationships $n_M = 1/(1-l_M)$ and $n = 1/(1-l)$ (van Genuchten, 1980) were assumed. The air-entry pressure values associated with S_{rM} were found to be approximately 9 MPa, a value considerably closer to those indicated for the macrostructure by other researchers, e.g., 0.5 MPa by Villar (2002) and 4.15 MPa by Alonso *et al*. (2011), than the values of 24-26 MPa identified for the parameter P of S_r (Table 5).

5. APPLICATION OF THE MODEL TO A SWELLING TEST

Given the relevance of the water flow in a swelling test, the analysis of a test of this type is a good method for illustrating the sensitivity of a water flow model to the use of differentiated definitions of water content. Nonetheless, the results of such an exercise depend not only on the adopted flux model but also on the stress-strain relationship applied. This influence is reduced by analysing an isotropic swelling test under constant mean stress, as that described in Section 2 (Fig. 3). In this case, after adopting the model for e_m defined by Eqs. 7, 8 and 16 and the parameters shown in Table 4, the deformation behaviour of the MX-80 in this type of isotropic test is determined by the model selected to define e_M. In this work, the same formulation as in the Barcelona Basic Model (Alonso *et al*., 1990), which is widely accepted for the simulation of the mechanical behaviour of bentonites (see, for instance, Lloret *et al*., 2003; Sánchez, *et al*., 2005; Gens *et al*., 2011; Guimarães *et al*., 2013; Navarro *et al*., 2014a), was used for modelling. The mechanical parameters of Table 6 were applied. With the exception of the initial net mean yield stress p_O^*, these parameters were obtained by fitting independent oedometric swelling tests performed by Sane *et al*. (2013) using the same MX-80 bentonite as that of the tests in Fig. 1. The value of p_O^*, 1800 kPa, was estimated from the pressure applied during the uniaxial compaction of the sample, 8059 kPa, using the proposal of Alonso *et al*. (2011).

In the numerical simulations, the gas pressure was assumed constant and equal to the atmospheric pressure (0.1 MPa) throughout the sample. As done for the microstructural suction (see Section 3), the osmotic component of the macrostructural suction was not taken into account, and $s=s_M$ was assumed. See Sedighi and Thomas, 2014, and references therein, for examples in which osmotic suction is taken into account. The lateral and upper surfaces were supposed to be impervious to water, and the liquid pressure at the base surface was taken as equal to atmospheric pressure. With respect to

the mechanical boundary conditions, a roller was applied to the sample base surface, and a normal pressure of 1.1 MPa was applied to the remaining boundaries, assuming isotropic strains.

Three different approaches were implemented in the partial differential equations solver defined in Section 3 to analyse the sensitivity of the flow model to the proposed water content models. In the first approach, which was adopted as a reference ("REF"), s_M was obtained with P_L, and S_{rM} was calculated using Eq. 17 and the parameters of Table 5. Moreover, Eqs. 7, 8 and 16 and the parameters of Table 4 allowed determination of s_m from e_m. In this analysis, the descriptions of the macrostructural and microstructural water content were considered separately, thus constituting a differentiated analysis. The modelled vertical swelling values in Fig. 11 and S_{rM} values in Fig. 12a were obtained. Even if available experimental water content values were desirable for a better validation of the model, the fit of the vertical swelling values illustrated in Fig. 11 provides confidence for the first approach implemented ("REF") as well as for the decision of adopting it as a reference. In addition, this satisfactory fit seems to confirm the validity of assuming an isotropic swelling behaviour (last paragraph of Section 3). Montes-Hernandez et al., 2006, describe a 21 MPa compaction pressure as "moderate", and thus it seems reasonable to use the same adjective to describe the 8059 kPa applied in this case, especially if compared to the compaction pressures of 50-100 MPa applied to MX-80 bentonites in other cases (see, among others, Johannesson and Börgesson, 1998; Johannesson, 2014; Börgesson and Hernelind, 2014). The compaction pressure applied was probably moderate enough to limit the anisotropy of the sample, not being large enough to invalidate the isotropic swelling hypothesis. Nevertheless, this hypothesis might not be valid for cases with a higher compaction pressure.

The "AP1" approach used the same mechanical model of the microstructure as that used in REF (Eqs. 7, 8 and 16 together with the parameters of Table 4). However, instead of using Eq. 17 to compute S_{rM}, its value was calculated from s_M using Eq. 18 ("mistakenly" identifying S_{rM} with S_r). Such calculations are performed when the contribution of the microstructural water content is ignored in the experimental determination of the soil characteristic curve. As a result, it is implicitly assumed that the entire soil water content derives from macrostructural water. Using this retention curve, the macrostructural water content is overestimated. To reduce this effect such that the water mass can be balanced, suction values greater than the real values are introduced in the calculations. Hence, using Eq. 17 in REF, a macrostructural initial suction of 25499 kPa was estimated for the initial conditions shown in Table 3, whereas the initial suction estimated using the AP1 approach and Eq. 18 was 44303 kPa. Because the initial suction is overestimated, a much larger final swelling was obtained (see Fig. 11). To obtain a "correct" swelling (equal to that of REF) from the simulation, an elastic stiffness for changes in suction (parameter κ_{So} in Table 6) of 0.01 should be adopted, which is significantly smaller than the reference value (0.05, Table 6). Such corrections could lead to important calculation errors in subsequent simulations with other geometries and boundary/initial conditions. In addition, even in the case under analysis, and although the final swelling is fitted with κ_{So}=0.01, the swelling evolution is not satisfactorily reproduced (Fig. 11).

These errors can be reduced by considering that S_{rM} and S_r are related by the following expression:

[19] $$S_{rM} = \frac{S_r \cdot (e_M + e_m - e_{mR}) - (e_m - e_{mR})}{e_M}$$

The third and last approach considered in this work, known as "AP2," was conducted in this manner by assuming that only Eq. 18 was determined experimentally. However, a differentiated procedure was adopted because the contribution of w_m in S_r was considered. The S_r was calculated using s_M and Eq. 18, and S_{rM} was subsequently deduced using Eq. 19. According to the data from Table 3, an initial suction value of 24127 kPa was estimated, which is similar to the value obtained in REF (25499 kPa). Therefore, the final swelling obtained with AP2 matches the swelling obtained with REF, which is shown in Fig. 11. Furthermore, the modelled evolutions of the swelling strains are practically identical and obtain overlapping curves (Fig. 11).

However, differences in the macrostructural degree of saturation are observed (Fig. 12a). In Fig. 12b, these differences are shown to be less than 20% and reach a maximum value at the base of the sample during the initial portion of the test; when the macrostructural suction gradients are greater, the advective flux of the macrostructural water is larger, and the time variation of s_M is faster. According to Eq. 3, s_m is equal to $p+s_M$ in the equilibrium; then, the sample experiences a situation farthest from the equilibrium between macrostructural and microstructural water at the base of the sample and at the beginning of the test, as illustrated in Fig. 13. However, the imbalance is practically negligible. It is thus valid to use Eq. 18, which was obtained under equilibrium conditions.

Situations further from equilibrium are produced if the transfer coefficient H increases from $1.5 \cdot 10^{-8}$ $(kPa \cdot s)^{-1}$ to $1.5 \cdot 10^{-11}$ $(kPa \cdot s)^{-1}$, the value identified by Alonso and Navarro (2005) in an analysis of the secondary compression of various clays. In this case, the difference between s_m and $p+s_M$ increases considerably at the base of the sample at the beginning of the test. Nonetheless, even in this case, the differences in the swelling strain between the REF and AP2 approaches are always less than 10 % (Fig. 14).

6. CONCLUSIONS

The aim of this work is to define a method for obtaining differentiated hydraulic models of the intra-aggregate (microstructural) and inter-aggregate (macrostructural) water content of MX-80 bentonite using data from water retention curves (WRCs). An additive (crystalline+osmotic swelling) approach is adopted to model the microstructural void ratio (Equation 7), obtaining noteworthy fittings for suctions greater than 20 MPa. For lower suction values, the additive model is extrapolated to estimate the microstructural water content. This way, the macrostructural water content is identified by subtracting the estimated microstructural water from the total water content experimental data. The WRCs obtained in this manner (Fig. 10) could be noticeably different from the total water content curves. If this difference is neglected and the macrostructural water content is modelled using retention curves corresponding to the total water content, excessively large values are obtained for the macrostructural suction. Therefore, to fit the swelling strains obtained experimentally, the soil stiffness for the changes in suction must be excessively reduced, which can lead to significant errors in the subsequent predictions of the bentonite behaviour.

To avoid these errors, it is advisable to separate the macrostructural water content from the total water content using Eq. 17. Nevertheless, it is also possible to use Eqs. 18 and 19 to differentiate the macrostructural degree of saturation. Eq. 18 is obtained under equilibrium conditions between macrostructural and microstructural water. Therefore, the validity of the latter procedure is constrained by the fulfilment of the equilibrium condition. For the analysed material, equilibrium is met, and therefore the two differentiated approaches (separate macro and micro water contents, either using Eq. 17 or using Eqs. 18 and 19 together) produce comparable results (Figs. 11, 12a and 12b).

These results are valid for the MX-80 bentonite analysed, but generalisation to other types of clay is by no means obvious. Note that only wetting paths have been analysed, and the dependence of the macrostructural water retention properties on the void ratio has not been considered (see Della Vecchia *et al*., 2014, and references therein). In addition, even if the results have shown a reduced sensitivity to the difference in density between free and adsorbed water in the cases analysed in the current work, the same might not apply in other cases (particularly for Ca-bentonites and for constant volume experiments). However, despite these limitations, this analysis illustrates the advisability of using differentiated approaches based on a double porosity retention model to characterise the behaviour of MX-80 bentonites.

ACKNOWLEDGEMENTS

This work was financed in part by B+Tech Oy (Finland) under a POSIVA Oy project. In addition, the authors gratefully acknowledge the financial support provided by the Spanish Ministry of Economy and Competitiveness under the Innocampus Program 2010. The authors also thank Oyinloye Femi Adesola and Oscar Merlo for collaboration in the experimental work conducted to obtain Figs. 1 and 3, respectively.

APPENDIX A. LIST OF SYMBOLS

A	Modulus of the Hamaker constant
B	Material parameter of the Δw_{mO} model
b	Material parameter
C	Parameter that describes the mass transfer change as s_{m} approaches s_{M}
c_m	Mass exchange term between macrostructural and microstructural water
e	Total void ratio
e_M	Macrostructural void ratio
e_m	Microstructural void ratio
e_{mC}	Microstructural void ratio associated with crystalline swelling
e_{mCMAX}	Microstructural void ratio associated with the crystalline swelling at saturation
e_{mR}	Additional microstructural void ratio
G_S	Specific gravity of the soil particles
g	Gravity constant
H	Parameter that defines the transfer coefficient at the end of the mass exchange process
K	Increase in cohesion with suction
k_{iM}	Isotropic intrinsic permeability
k_{MO}	Intrinsic permeability when the macrostructural porosity is ϕ_{MO}
k_{rM}	Relative permeability
l	Fitting parameter of S_{r}
l_M	Fitting parameter of S_{rM}

l_m	Fitting parameter of e_{mC}
M	Slope of the critical state line
M_w	Molar mass of water
m_M	Mass of macrostructural water per unit volume
m_m	Mass of microstructural water per unit volume
n	Fitting parameter of S_r
n_m	Fitting parameter of e_{mC}
P	Total air-entry pressure value
P_{ATM}	Atmospheric pressure
P_G	Gas pressure
P_L	Pressure of macrostructural liquid
P_M	Macrostructural air-entry pressure value
p	Net mean stress
p_C	Reference stress
p_O^*	Initial net mean yield stress
p_{REF}	Material parameter used to define κ_S
p_{TOT}	Mean stress
$\boldsymbol{q}_M$	Macrostructural water seepage
R	Universal gas constant
RH	Relative humidity
r	Material parameter used to define the macrostructural soil compressibility
S	Clay specific surface area
S_{mO}	Microstructural suction at which osmotic swelling begins to play a significant role

S_r	Total degree of saturation
S_{rM}	Macrostructural degree of saturation
s	Total suction
s_f	Final total suction
s_M	Macrostructural matric suction
s_m	Microstructural suction
s_o	Initial value of total suction
T	Absolute temperature
t	Approximate thickness of an adsorbed water layer
t_s	Approximate thickness of a montmorillonite sheet
w	Total water content
w_f	Water content at equilibrium with the final total suction s_f
w_M	Macrostructural water content
w_m	Microstructural water content
w_{mC}	Crystalline microstructural water content
w_o	Initial value of water content
z	Vertical coordinate
α_i	Material parameter used to define κ
α_m	Fitting parameter of e_{mC}
α_{Sp}	Material parameter used to define κ_S
α_{SS}	Material parameter used to define κ_S
β	Material parameter used to define the macrostructural soil compressibility
Δe_{mO}	Increase in microstructural void ratio caused by osmotic swelling

Δw_{mO}	Increase in microstructural water content caused by osmotic swelling
ε_v	Volumetric strain
ε_z	Axial (vertical) strain
κ_{io}	Material parameter used to define the macrostructural elastic stiffness for changes in net mean stress (κ)
κ_m	Microstructural stiffness parameter
κ_{So}	Material parameter used to define the macrostructural elastic stiffness for changes in suction (κ_S)
$\lambda(0)$	Slope of the virgin compression curve for saturated conditions
μ_W	Dynamic viscosity of water
ν	Poisson's ratio
ρ_d	Dry density
ρ_n	Bulk density
ρ_s	Density of mineral particles
ρ_W	Free water density
ρ_{Wm}	Microstructural water density
ϕ_M	Macrostructural porosity
ϕ_{MO}	Reference macrostructural porosity
$\partial/\partial t$	Time derivative
$\nabla\cdot$	Divergence operator
∇	Gradient operator

526

REFERENCES

Alonso E.E. and Navarro V. (2005) Microstructural model for delayed deformation of clay: loading history effects. Can Geotech J 42(2):381-392

Alonso E.E., Gens A., Josa A. (1990) A constitutive model for partially saturated soils. Géotechnique 40(3):405-430

Alonso E.E., Gens A., Lloret A. (1991). Double structure model for the prediction of long-term movements in expansive materials. In: Beer G., Booker J.R., Carter J.P. (eds.) Computer methods and advances in geomechanics, vol. 1, pp. 541–548. Rotterdam, The Netherlands: Balkema

Alonso E.E., Vaunat J., Gens A. (1999). Modelling the mechanical behaviour of expansive clays. Eng Geol 54(1–2):173–183

Alonso E. E., Romero E., Hoffmann C. (2011) Hydromechanical behaviour of compacted granular expansive mixtures: experimental and constitutive study. Géotechnique 61(4):329–344. DOI: 10.1680/geot.2011.61.4.329

ASTM (2010). ASTM D2216-10, Standard Test Methods for Laboratory Determination of Water (Moisture) Content of Soil and Rock by Mass, ASTM International, West Conshohocken, PA. DOI: 10.1520/D2216-10

Barshad I. (1955) Adsorptive and swelling properties of clay-water system. In: Pask J.A. and Turner M.D. (eds.) Proceedings of Clays and clay technology: 1st National Conference on Clays and Clay Technology. Berkeley, California, July 21-25 1952. California Division of Mines Bulletin 169. p. 70-77.

Börgesson L. and Hernelind J. (1999) Äspö Hard Rock Laboratory. Prototype Repository. Preliminary modelling of the water saturation phase of the buffer and backfill materials. SKB, International Progress Report IPR-00-11. Swedish Nuclear Fuel and Waste Management Co. Available at: skb.se/upload/publications/pdf/ipr-00-11.pdf, last accessed July 2015

Börgesson L. and Hernelind J. (2014) Modelling of bentonite block compaction. SKB, Report P-14-10. Swedish Nuclear Fuel and Waste Management Co. Available at: www.skb.com/publication/2719608/, last accessed October 2015

Bourg I.C., Sposito G., Bourg A.C.M. (2006) Tracer diffusion in compacted, water-saturated bentonite. Clay Clay Miner 54(3):363-374.

Brooks R.M. and Corey A.T. (1964). Hydraulic properties of porous media. Hydrology Paper no. 3. Fort Collins, Colorado, USA: Colorado State University

Burdine N.T. (1953). Relative permeability calculations from pore size distribution data. Trans Am Inst Mining Metall Eng 198:71-78

Cases J.M., Bérend I., Besson G., François M., Uriot J.P., Thomas F., Poirier J.E. (1992) Mechanism of Adsorption and Desorption of Water Vapor by Homoionic Montmorillonite. 1. The Sodium-Exchanged Form. Langmuir 8:2730-2739

Casini F., Vaunat J., Romero E., Desideri A. (2012) Consequences on water retention properties of double-porosity features in a compacted silt. Acta Geotech 7:139–150. DOI: 10.1007/s11440-012-0159-6

Comsol AB. (2011) COMSOL Multiphysics Reference Guide, version 4.2. COMSOL

Delage P. (2002) Experimental unsaturated soil mechanics: State-of-the-art report. In: Juca JFT, De Campos TMP, Marino FAM (eds.) Proc. 3rd Int. Conf. on Unsaturated Soils UNSAT'2002 (3):973-996. Recife, Brazil: Balkema

Delage P., Audiguier M., Cui Y.J., Howat M.D. (1996) Microstructure of a compacted silt. Can Geotech J 33(1):150–158

Delage P., Marcial D., Cui Y.J., Ruiz X. (2006) Ageing effects in a compacted bentonite: a microstructure approach. Géotechnique 56(5):291–304

Delage P., Romero E., Tarantino A. (2008) Recent developments in the techniques of controlling and measuring suction in unsaturated soils. Proc. 1st Eur. Conf. on Unsaturated Soils, 33-52, E-UNSAT 2008, Durham, United Kingdom

Della Vecchia G., Jommi C., Romero E. (2012) A fully coupled elastic–plastic hydromechanical model for compacted soils accounting for clay activity. Int J Numer Anal Methods Geomech 37(5):503–535

Della Vecchia G., Dieudonné A.C., Jommi C., Charlier R. (2014) Accounting for evolving pore size distribution in water retention models for compacted clay. Int J Numer Anal Methods Geomech. DOI: 10.1002/nag.2326

Dueck A. (2004) Hydro-mechanical properties of a water unsaturated sodium bentonite. Laboratory study and theoretical interpretation. Ph. D. Thesis, Lund University. Sweden

Dueck A. (2008) Laboratory results from hydro-mechanical tests on a water unsaturated bentonite. Eng Geol 97(1-2):15–24

Dueck A. and Börgesson L. (2007) Model suggested for an important part of the hydro-mechanical behaviour of a water unsaturated bentonite. Eng Geol 92:160–169

Dueck A. and Nilsson U. (2010) Thermo-Hydro-Mechanical properties of MX-80. Results from advanced laboratory tests. SKB Technical Report TR-10-55. Swedish Nuclear Fuel and Waste Management Co. Available at: www.skb.se/upload/publications/pdf/TR-10-55.pdf, last accessed July 2015

Durner W. (1994) Hydraulic conductivity estimation for soils with heterogeneous pore structure. Water Resour Res 30(2):211-223

Edlefsen N.E. and Anderson A.B.C. (1943) Thermodynamics of soil moisture. Hilgardia 15(2):31-298

Enresa (2000) FEBEX project. Full-scale engineered barriers experiment for a deep geological repository for high level radioactive waste in crystalline host rock. Final Report. PT 01/00. Madrid, Spain: Empresa Nacional de Residuos Radioactivos. Available at: www.enresa.es/publicaciones_y_audiovisuales/documentacion/pdf_febex_project_full, last accessed July 2015

Gee G.W., Campbell M.D., Campbell G.S., Campbell J.H. (1992) Rapid measurement of low soil water potentials using a water activity meter. Soil Sci Soc Am J 56:1068–1070

Gens A. and Alonso E.E. (1992) A framework for the behavior of unsaturated expansive clays. Can Geotech J 29(6):1013–1032

Gens A., Valleján B., Sánchez M., Imbert C., Villar M.V., Van Geet M. (2011) Hydromechanical behaviour of a heterogeneous compacted soil: experimental observations and modelling. Géotechnique 61(5): 367-386. DOI: 10.1680/geot.SIP11.P.015

Gerke H.H. and van Genuchten M.T. (1993a) A dual-porosity model for simulating the preferential movement of water and solutes in structured porous media. Water Resour Res 29(2):305-319

Gerke H.H. and van Genuchten M.T. (1993b) Evaluation of a first-order water transfer term for variably saturated dual-porosity flow models. Water Resour Res 29(4):1225-1238

Ghafouri H.R. and Lewis R.W. (1996) A finite element double porosity model for heterogeneous deformable porous media. Int J Numer Anal Methods Geomech 20(11):831-844

Guimarães L.N., Gens A., Sánchez M., Olivella S. (2013). A chemo-mechanical constitutive model accounting for cation exchange in expansive clays. Géotechnique 63(3):221–234. DOI: 10.1680/geot.SIP13.P.012

Hueckel T.A. (1992) Water-mineral interaction in hygromechanics of clays exposed to environmental loads: a mixture-theory approach. Can Geotech J 29(6):1071-1086

Jacinto A.C., Villar M.V., Gómez-Espina R., Ledesma A. (2009) Adaptation of the van Genuchten expression to the effects of temperature and density for compacted bentonites. Appl Clay Sci 42:575–582

Jacinto A.C., Villar M.V., Ledesma A. (2012) Influence of water density on the water-retention curve of expansive clays. Géotechnique 62(8):657–667

Johannesson L-E., Börgesson L. (1998) Compaction of bentonite blocks. Development of techniques for production of blocks with different shapes and sizes. SKB, Report R-99-12. Swedish Nuclear Fuel and Waste Management Co. Available at: www.skb.se/upload/publications/pdf/R-99-12.pdf, last accessed October 2015

Johannesson L-E. (2014) Manufacturing of buffer and filling components for the Multi Purpose Test. SKB, Report P-14-07. Swedish Nuclear Fuel and Waste Management Co. Available at: www.skb.se/upload/publications/pdf/P-14-07.pdf, last accessed October 2015

Kahr G., Kraehenbuehl F., Stoeckli H.F., Müller-Vonmoos M. (1990) Study of the water-bentonite system by vapour adsorption, immersion calorimetry and X-ray techniques: II. Heats of immersion, swelling pressures and thermodynamic properties. Clay Miner 25:499–506

Karnland O., Olsson S., Nilsson U. (2006) Mineralogy and sealing properties of various bentonites and smectite-rich clay minerals. SKB Technical Report TR-06-30. Swedish Nuclear Fuel and Waste Management Co. Available at: www.skb.se/upload/publications/pdf/TR-06-30.pdf, last accessed July 2015

Kumpulainen S. and Kiviranta L. (2010) Mineralogical and chemical characterization of various bentonite and smectite-rich clay materials. Part A: Comparison and development of mineralogical characterization methods. Part B: Mineralogical and chemical characterization of clay materials. Posiva Working Report 2010-52. Available at: www.posiva.fi/files/3098/WR_2010-52_Korjattu_17.6.13.pdf, last accessed July 2015

Laird D.A. (1996) Model for crystalline swelling of 2:1 phyllosilicates. Clay Clay Miner 44(4):553-559

Leong E.C., Tripathy, S., Rahardjo H. (2003) Total suction measurement of unsaturated soils with a device using chilled-mirror dew-point technique. Gèotechnique 53(2): 173-182

Lloret A., Villar M.V., Sánchez M., Gens A., Pintado X., Alonso E.E. (2003) Mechanical behaviour of heavily compacted bentonite under high suction changes. Géotechnique 53(1):27–40

Low P.F. (1987) Structural component of the swelling pressure of clays. Langmuir 3(1):18–25. DOI: 10.1021/la00073a004

Montes-H G., Duplay, J. Martinez, L. Mendoza, C. (2003) Swelling–shrinkage kinetics of MX80 bentonite. Appl Clay Sci 22(6): 279–293

Montes-Hernandez G., Duplay J., Géraud Y., Martinez L. (2006) Several textural properties of compacted and cation-exchanged bentonite. J Phys Chem Solids 67(8): 1769-1174

Musso G., Romero E., Della Vecchia G. (2013) Double structure effects on the chemo-hydro-mechanical behaviour of compacted active clay. Géotechnique 63(3):206-220. DOI: 10.1680/geot.SIP13.P.011

Navarro V., Barrientos V., Yustres Á., Delgado J. (2008) Settlement of embankment fills constructed of granite fines. Comput Geosci 34(8):978–992

Navarro V., Asensio L., Yustres Á., Pintado X., Alonso J. (2013) Volumetric deformability and water mass exchange of bentonite aggregates. Eng Geol. DOI: 10.1016/j.enggeo.2013.09.011

Navarro V., Asensio L., Yustres Á., Pintado X., Alonso J. (2014a) An elastoplastic model of bentonite free swelling. Eng Geol 181:190-201. DOI: 10.1016/j.enggeo.2014.07.014

Navarro V., Asensio L., Alonso J., Yustres Á., Pintado X. (2014b) Multiphysics implementation of advanced soil mechanics models. Comput Geotech 60:20–28. DOI: 10.1016/j.compgeo.2014.03.012

Neretnieks I., Liu L., Moreno L. (2009) Mechanisms and models for bentonite erosion. SKB Technical Report TR-09-35. Svensk Kärnbränslehantering AB, Swedish Nuclear Fuel and Waste Management Co. Available at: www.skb.se/upload/publications/pdf/TR-09-35.pdf, last accessed July 2015Or D. and Tuller M. (1999) Liquid retention and interfacial area in variably saturated porous media: Upscaling from single-pore to sample-scale model. Water Resour Res 35(12):3591– 3606

Pintado X., Lloret A., Romero E. (2009) Assessment of the use of the vapour equilibrium technique in controlled-suction tests. Can Geotech J 46(4):411

Pintado X., Mamunul H.M., Martikainen J. (2013) Thermo-hydro-mechanical tests of buffer material. Posiva Working Report 2012-49. Available at: www.posiva.fi/files/3385/POSIVA_2012-49.pdf, last accessed July 2015

Pusch R. (1983) Stability of bentonite gels in crystalline rock. Physical aspects. SKBF-KBS Technical Report TR-83-04. Svensk Kärnbraänsleförsörjning AB/ Avdelning

KBS. Available at: www.skb.se/upload/publications/pdf/TR83-04webb.pdf, last accessed July 2015

Pusch R., Karnland O., Hökmark H. (1990) GMM - A general microstructural model for qualitative and quantitative studies of smectite clays. SKB Technical Report TR-90-43. Svensk Kärnbränslehantering AB; Swedish Nuclear Fuel and Waste Management Co. Available at: www.skb.se/upload/publications/pdf/TR90-43_inlaga.pdf, last accessed July 2015.

Romero E., Gens A., Lloret A. (1999) Water permeability, water retention and microstructure of unsaturated compacted Boom clay. Eng Geol 54(1-2):117-127

Romero E., Della Vecchia G., Jommi C. (2011) An insight into the water retention properties of compacted clayey soils. Géotechnique 61(4):313–328. DOI: 10.1680/geot.2011.61.4.313

Salas J.D., Delleur J.W., Yevjevich V.M., Lane, W.L. (1980) Applied modeling of hydrologic time series. Water Resources Publications, 484 pp, Littleton, Colorado

Salles F., Douillard J.M., Denoyel R., Bildstein O., Jullien M., Beurroies I., van Dammed H. (2009) Hydration sequence of swelling clays: Evolutions of specific surface area and hydration energy. J Colloid Interface Sci 333:510–522

Sánchez M., Gens A., Guimarães L.N., Olivella S. (2005) A double structure generalized plasticity model for expansive materials. Int J Numer Anal Methods Geomech 29(8):751–787

Sane P., Laurila T., Olin M., Koskinen K. (2013) Current status of mechanical erosion studies of bentonite buffer. Posiva Report 2012-45. Available at: www.posiva.fi/files/3349/POSIVA_2012-45.pdf, last accessed October 2015.

Sedighi M. and Thomas H.W. (2014) Micro porosity evolution in compacted swelling clays-A chemical approach. Appl Clay Sci 101:608–618

Sposito G. and Prost R. (1982) Structure of water adsorbed on smectites. Chem Rev 82(6):553-573

Tournassat C. and Appelo C.A.J. (2011) Modelling approaches for anion-exclusion in compacted Na-bentonite. Geochim Cosmochim Acta 75(13):3698-3710

Tuller M. and Or D. (2005) Water films and scaling of soil characteristic curves at low water contents. Water Resour Res 41, W09403. DOI:10.1029/2005WR004142

van Genuchten M.T. (1980) A closed-form equation for predicting the hydraulic conductivity of unsaturated soils. Soil Sci Soc Am J 44(5):892–898

van Genutchen M.T. and Wierenga P.J. (1976) Mass transfer studies in sorbing porous media I. Analytical solutions. Soil Sci Soc Am J 40(4):473-480

Villar M.V. (2002) Thermo-hydro-mechanical characterisation of a bentonite from Cabo de Gata. A study applied to the use of bentonite as sealing material in high level radioactive waste repositories. PT 04/02. Madrid, Spain: Empresa Nacional de Residuos Radioactivos. Available at: www.enresa.es/files/multimedios/PT04-02.pdf, last accessed July 2015

Villar M.V. (2007) Water retention of two natural compacted bentonites. Clay Clay Miner 55(3):311–322

Wadsö L., Svennberg K., Dueck A. (2004) An experimentally simple method for measuring sorption isotherms. Dry Technol 22:2427–2440

Wilson R. and Aifantis E. (1982) On the theory of consolidation with double porosity. Int J Eng Sci 20(9)1009–1035

Yahia-Aïssa M. (1999) Comportement hydromécanique d'une argile gonflante fortement compactée. PhD Thesis. École Nationale des Ponts et Chaussées, Paris, France

Table 1. Main properties of the MX-80 bentonite batches studied in this work. Data from Kumpulainen and Kiviranta (2010).

	Volclay MX-80	**Wym**
Smectite	76.3	81.4
Illite	1.8	0.8
Calcite	0.7	0.2
Cristobalite	0.6	0.2
Gypsum	1.2	0.9
Hematite	0.4	0.4
Plagioclase	2.3	3.5
Pyrite	0.8	0.6
Quartz	4.8	3.0
CEC (eq/kg)	0.89	0.86
Na^+ / K^+ / Ca^{2+} / Mg^{2+} (eq/kg)	0.60 / 0.02 / 0.19 / 0.07	0.74 / 0.02 / 0.18 / 0.07
Grain density g/cm^3	2.78	2.78

Table 2. Tests conducted by B+Tech (Pintado *et al.*, 2013). Symbols w_o and s_o define the initial water content and total suction values, respectively; $_d$ is the water content and w_f is the water content at equilibrium with the final total suction s_f.

Test ID	w_o (%)	s_o (MPa)	$_d$ (kg/m^3)	w_f (%)	s_f (MPa)
091218a	6.2	204.1	1576	3.0	288.1
			1682	3.3	287.9
			1522	10.6	89.4
			1530	16.0	54.2
			1529	15.0	60.9
			1544	24.9	13.3
100111b	4.6	263.0	1622	3.1	267.5
			1587	3.6	254.7
			1543	9.5	95.9
			1510	12.7	71.1
			1539	13.3	68.6
			1472	16.9	44.9
100208a	5.1	204.8	1655	4.2	270.2
			1661	6.7	177.0
			1461	9.6	101.8
			1446	15.7	56.9
			1559	11.2	79.1
			1576	20.8	25.5
100222a	5.5	231.9	1589	8.6	99.7
			1638	11.1	80.4
			1578	13.2	71.7
			1539	15.1	56.6
			1580	18.0	40.4
			1603	19.6	28.1

Table 3. Initial conditions of the MX-80 sample used in the isotropic swelling test.

w (%)	20
$_{n}$ (g/cm^3)	2.03
$_{d}$ (g/cm^3)	1.692
e	0.646
S_r	0.868

Table 4. Parameters identified to characterise the microstructural void ratio using the data of Fig. 2.

e_{mR}	0.093
e_{mCMAX}	0.480
α_m (MPa^{-1})	0.016
l_m	0.612
$_m$	0.04
s_{mO} (MPa)	40

Table 5. Parameters identified to characterise Sr_M and Sr.

P_M (MPa)	8.70
l_M	0.73
P (MPa)	26.58
l	0.43

Table 6. Parameters of the Barcelona Basic Model for the MX-80 analysed in this work.

Parameter	Value
K	0.1
$_{io}$	0.1
$_{i}$ (1/kPa)	0
$_{So}$	0.05
$_{Sp}$	0
$_{SS}$ (1/kPa)	0
p_{REF} (kPa)	10
	0.35
p_C (kPa)	10
(0)	0.15
r	0.8
(1/kPa)	$2.0 \cdot 10^{-5}$
p_O^* (kPa)	1800
M	1.07

Figure 1

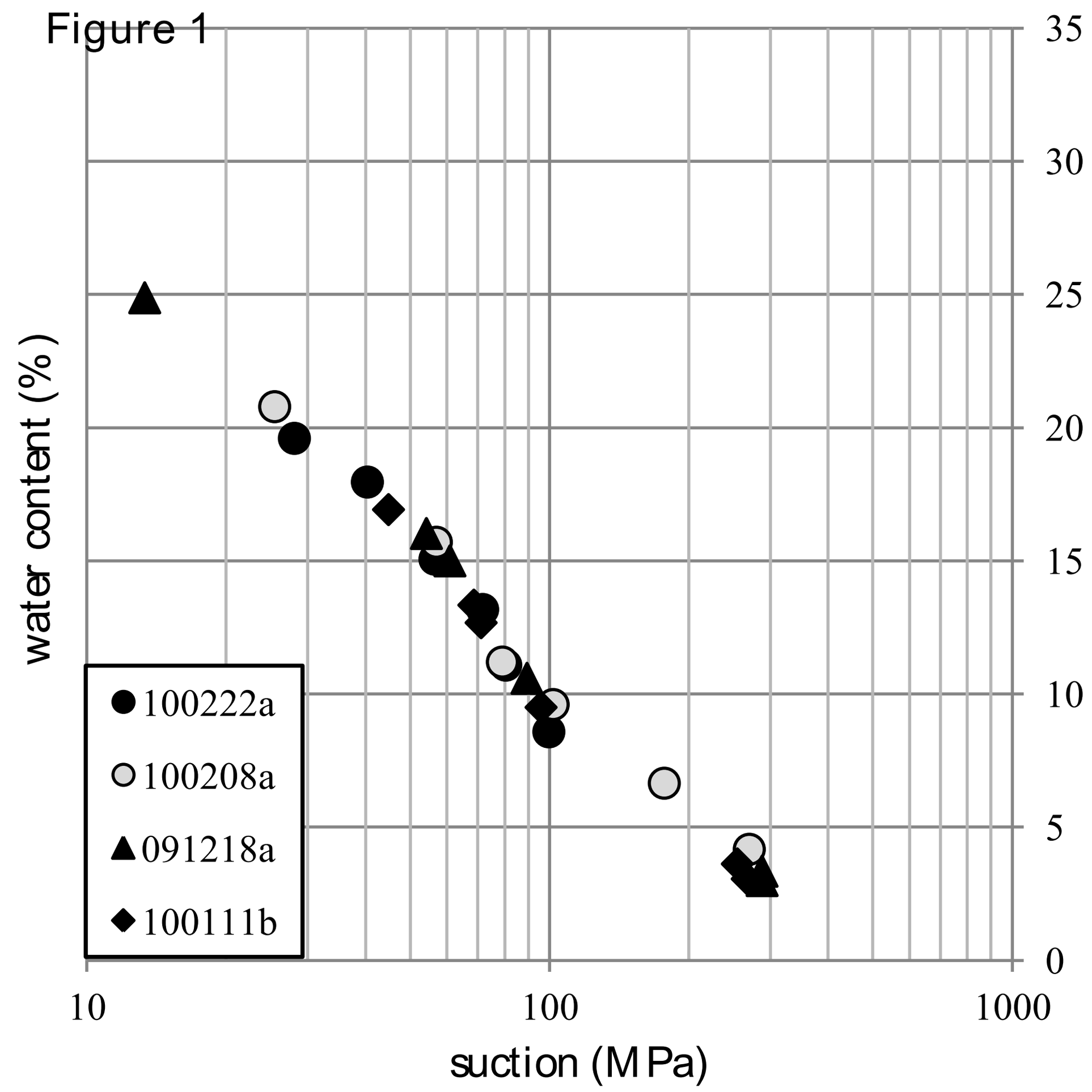
water content (%)
35
30
25
20
15
10
5
0
10
100
1000
suction (MPa)
100222a
100208a
091218a
100111b

Figure 2

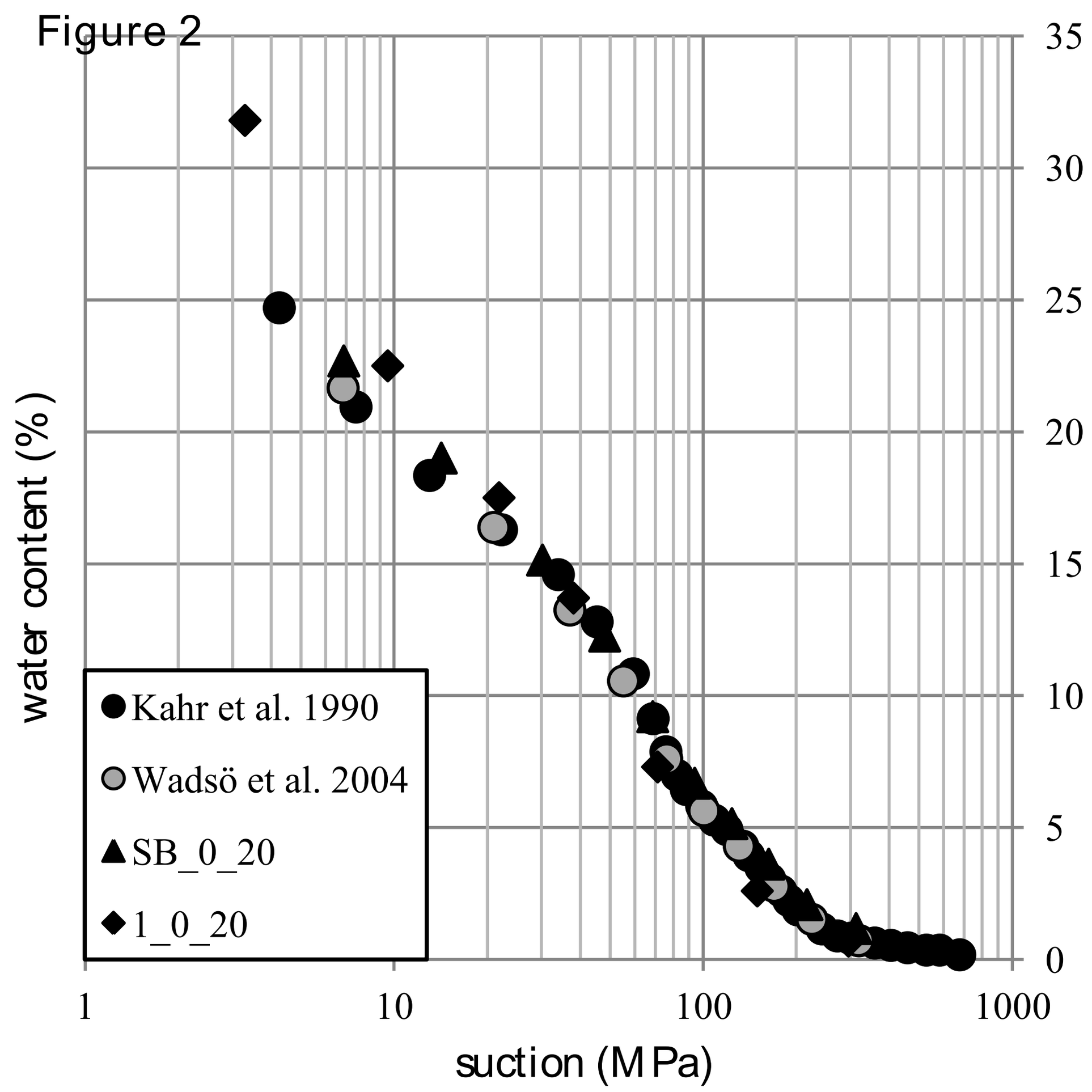
35
30
25
20
15
10
5
0
water content (%)
Kahr et al. 1990
Wadsö et al. 2004
SB_0_20
1_0_20
1
10
100
1000
suction (MPa)

Figure 3

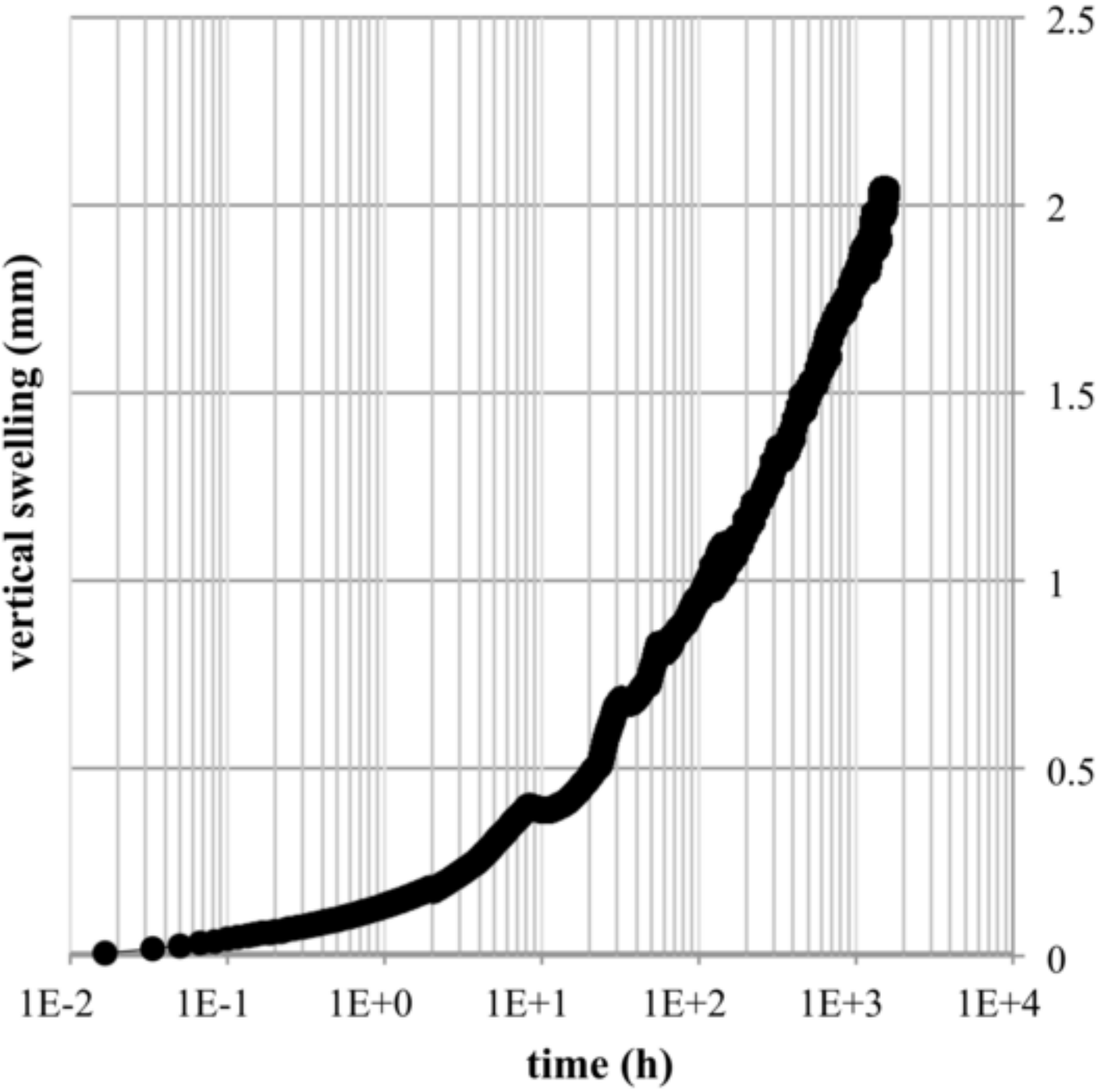
vertical swelling (mm)
2.5
2
1.5
1
0.5
0
1E-2
1E-1
1E+0
1E+1
1E+2
1E+3
1E+4
time (h)

Figure 4

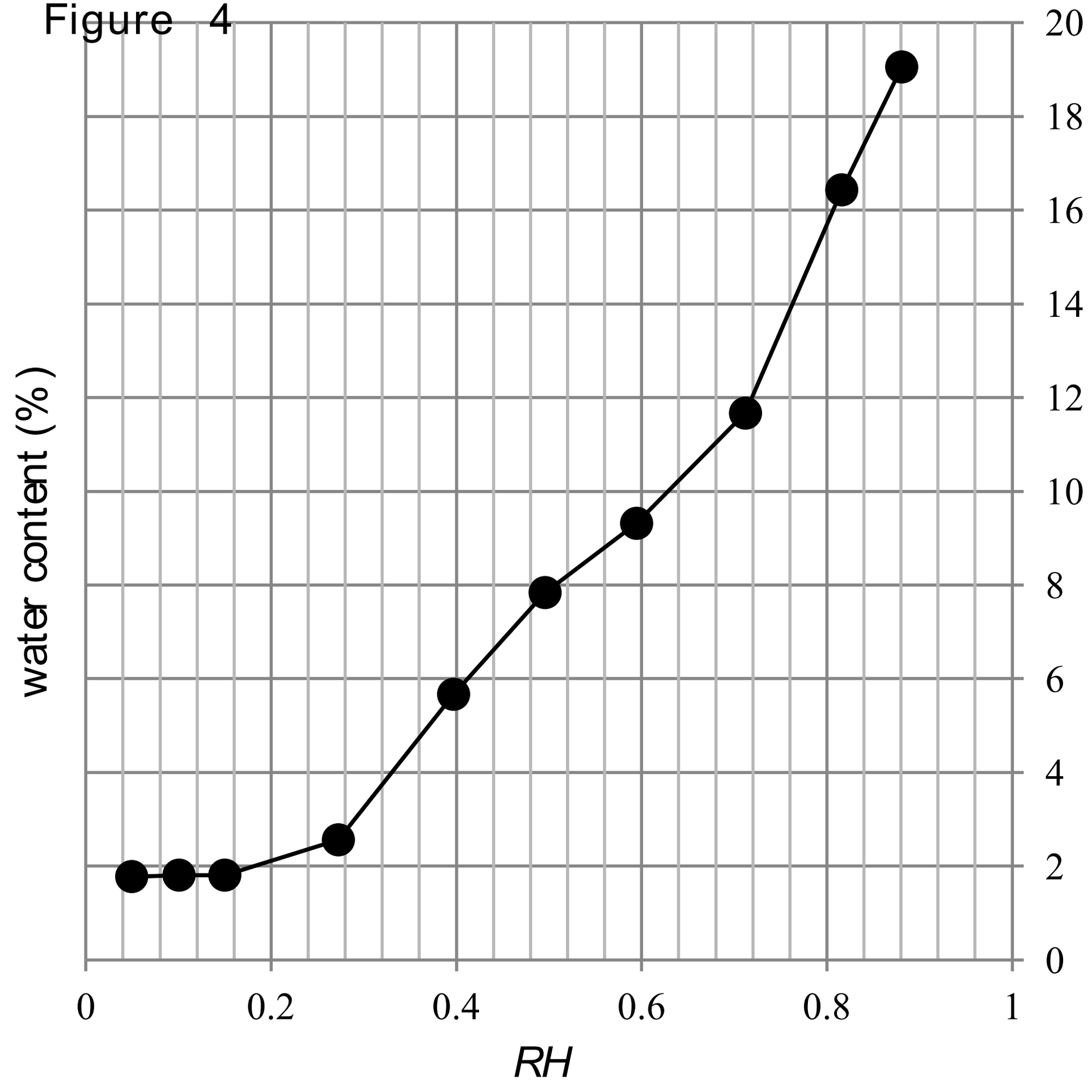

Figure 5

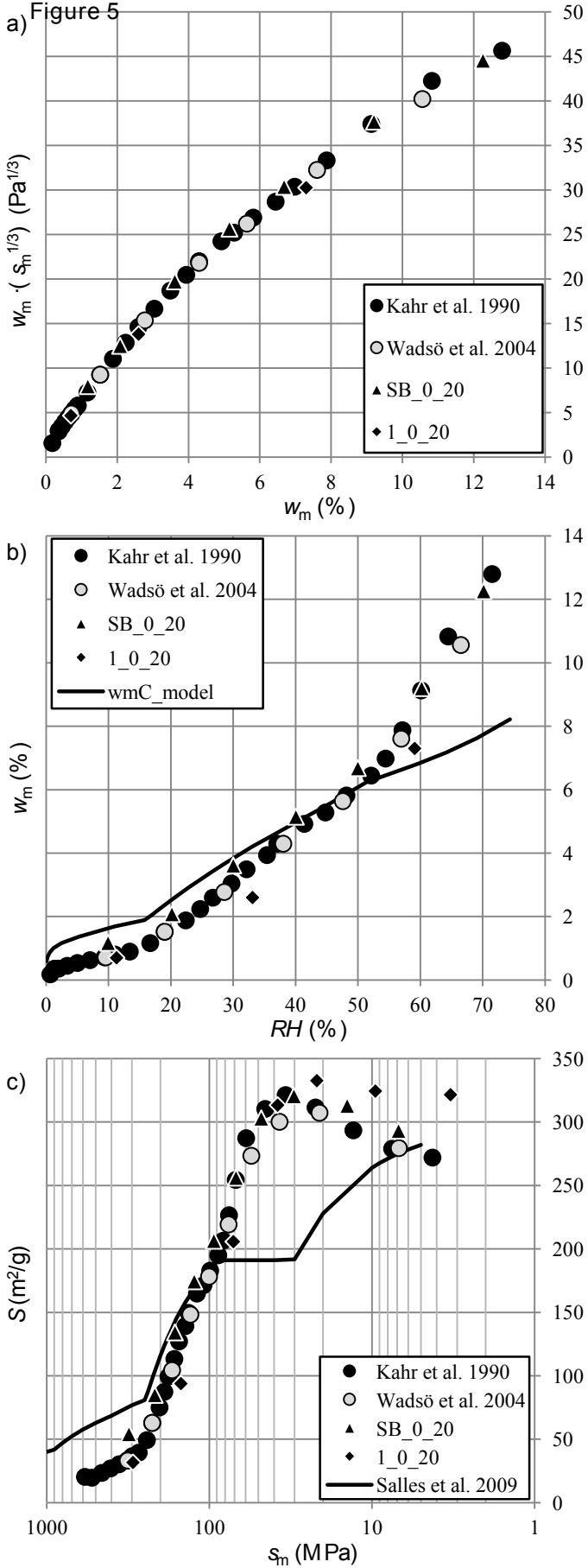
a)
$w_m \cdot (s_m^{1/3})$ (Pa$^{1/3}$)
w_m (%)
Kahr et al. 1990
Wadsö et al. 2004
SB_0_20
1_0_20
b)
w_m (%)
RH (%)
Kahr et al. 1990
Wadsö et al. 2004
SB_0_20
1_0_20
wmC_model
c)
S (m^2/g)
s_m (MPa)
Kahr et al. 1990
Wadsö et al. 2004
SB_0_20
1_0_20
Salles et al. 2009

Figure 6

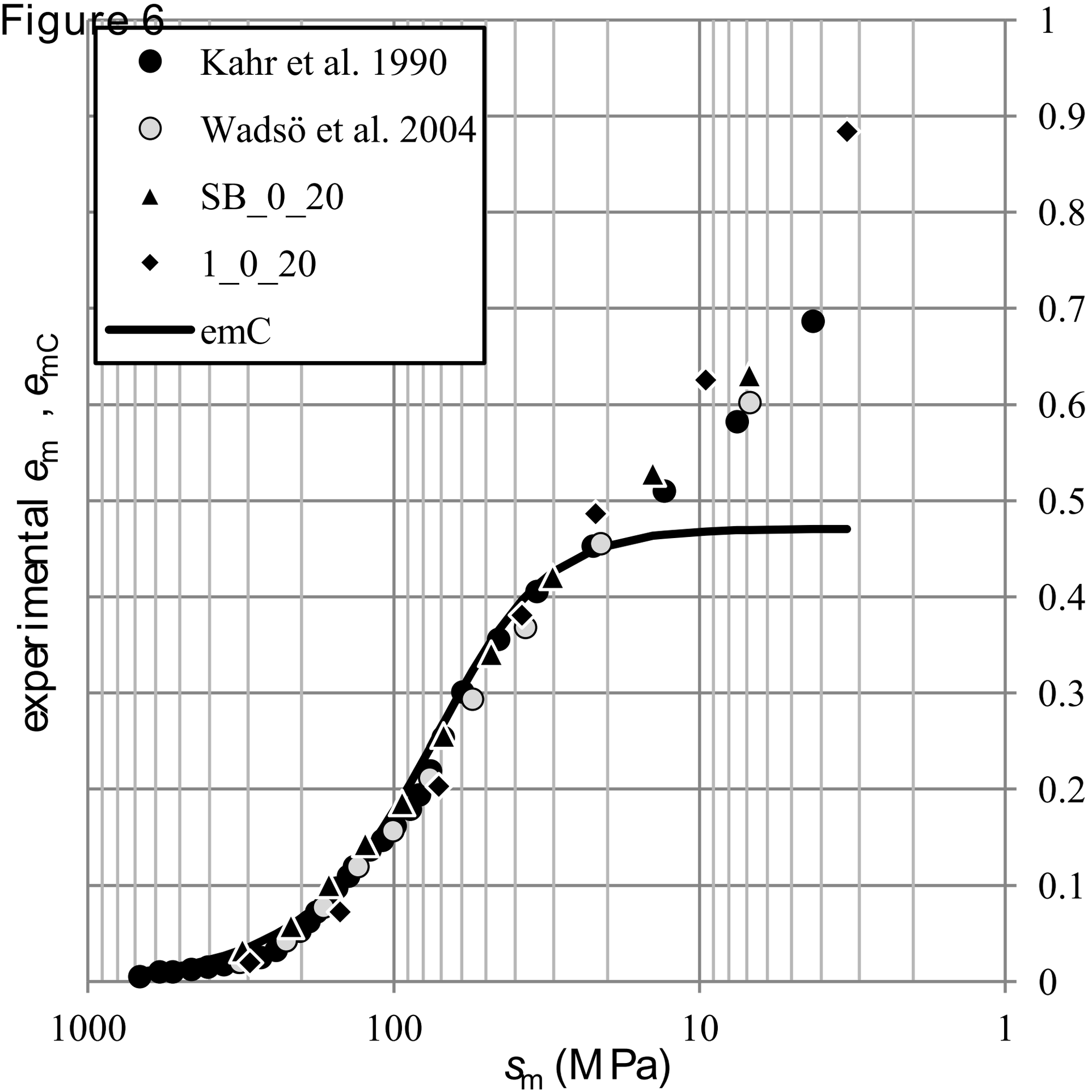
Kahr et al. 1990
Wadsö et al. 2004
SB_0_20
1_0_20
emC
experimental e_m , e_{mC}
1
0.9
0.8
0.7
0.6
0.5
0.4
0.3
0.2
0.1
0
1000
100
10
1
s_m (MPa)

Figure 7

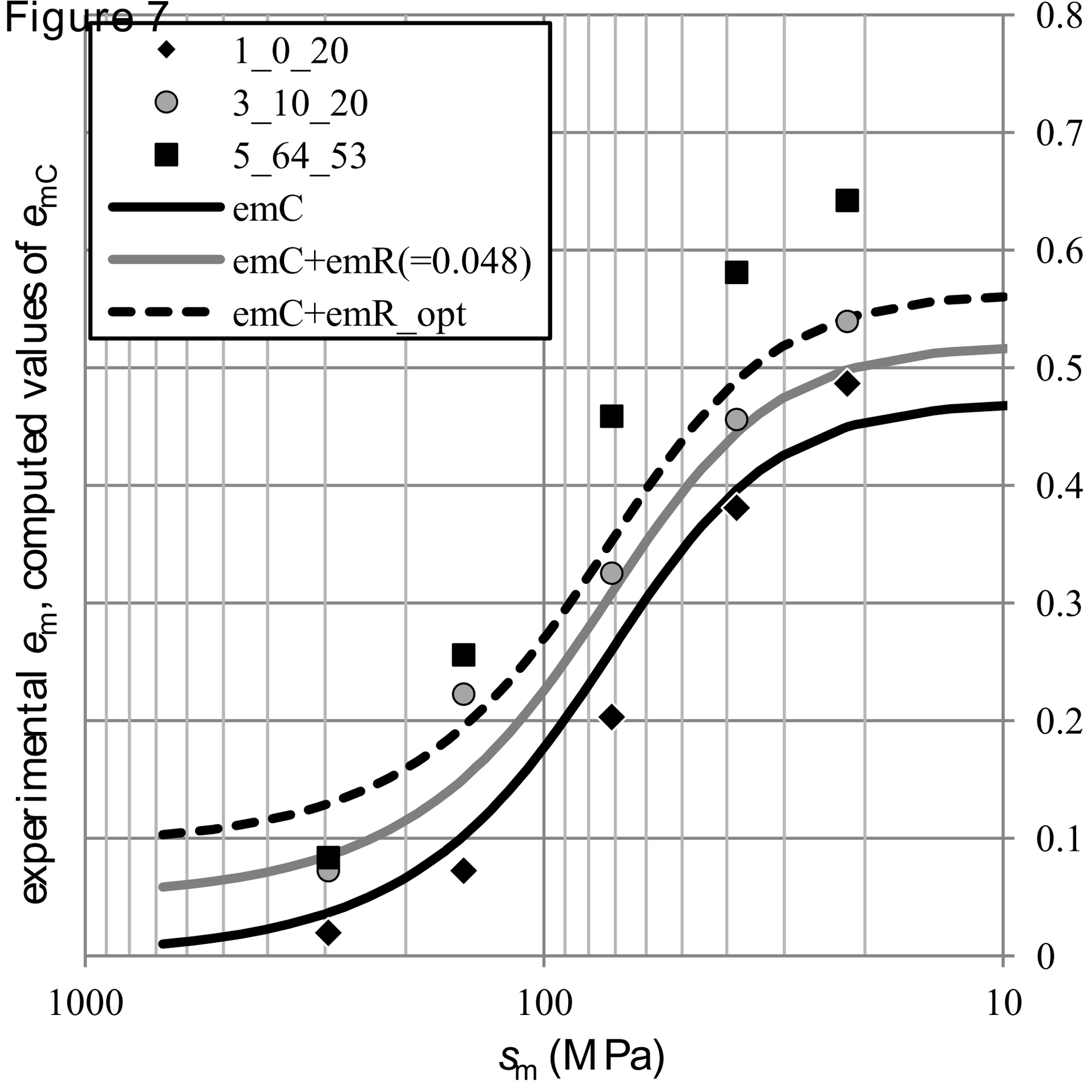
1_0_20
3_10_20
5_64_53
emC
emC+emR(=0.048)
emC+emR_opt
experimental e_m, computed values of e_{mC}
0.8
0.7
0.6
0.5
0.4
0.3
0.2
0.1
0
1000
100
10
s_m (MPa)

Figure 8

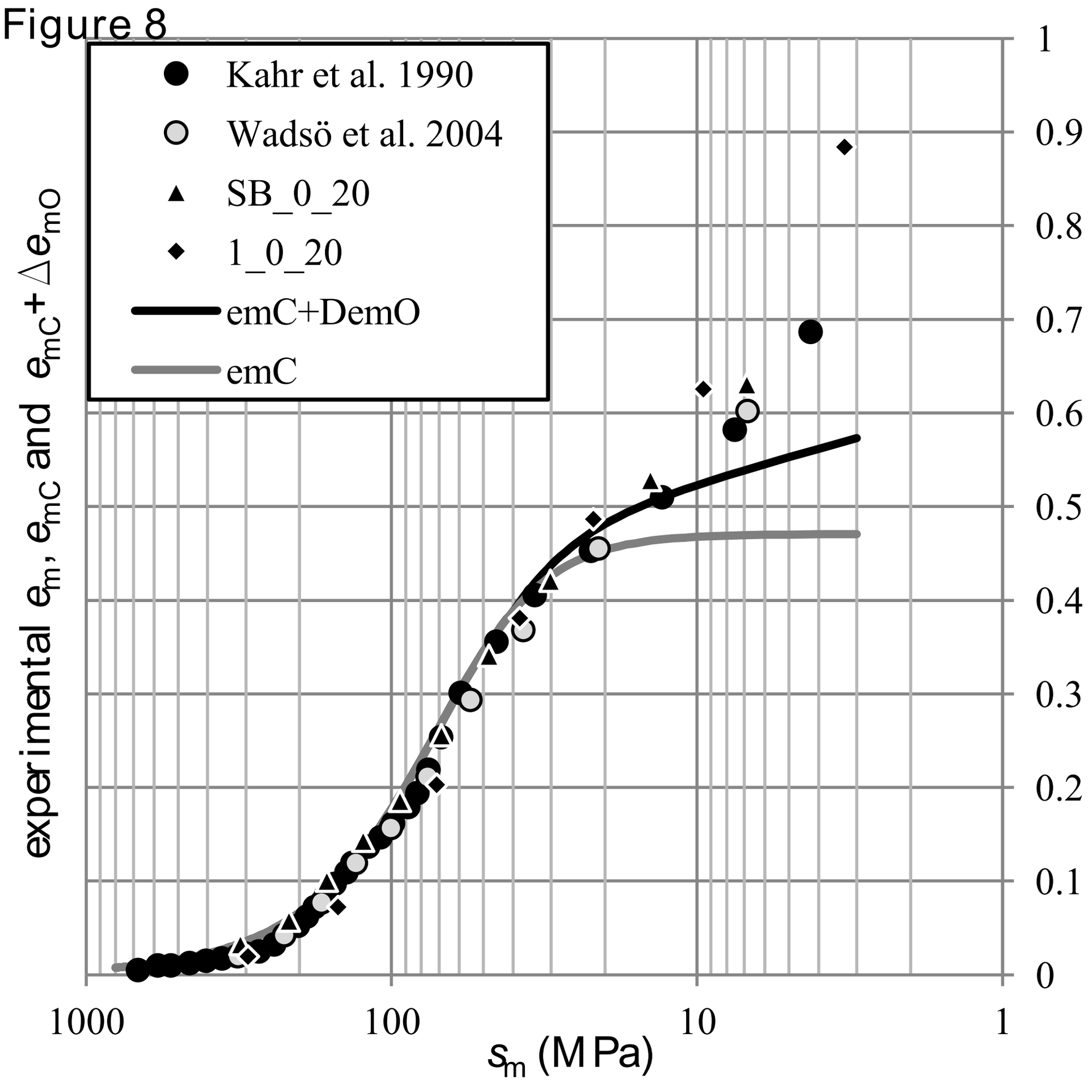
Kahr et al. 1990
Wadsö et al. 2004
SB_0_20
1_0_20
emC+DemO
emC
experimental e_m, e_{mC} and $e_{mC}+\Delta e_{mO}$
s_m (MPa)
1000
100
10
1
0
0.1
0.2
0.3
0.4
0.5
0.6
0.7
0.8
0.9
1

Figure 9

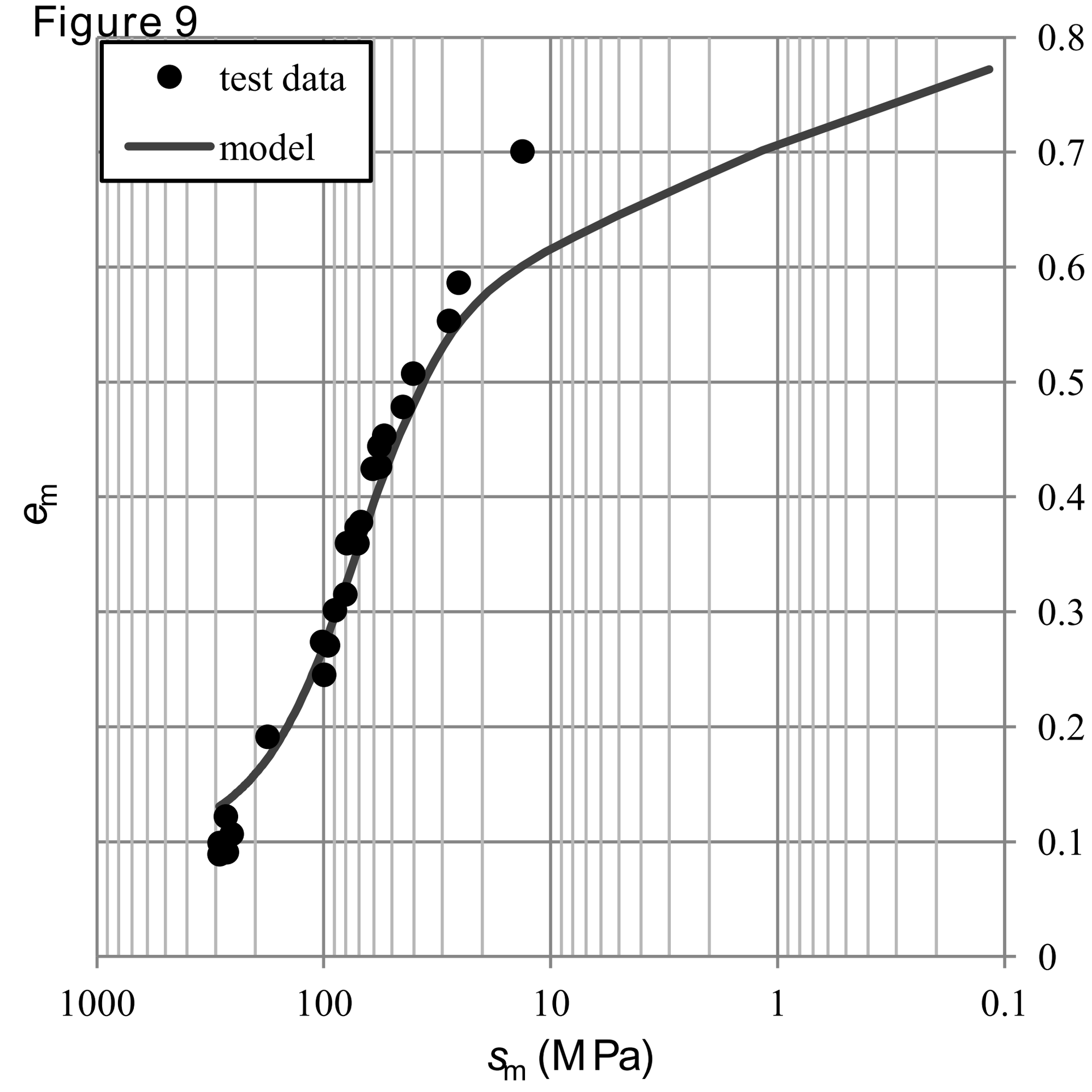

Figure 10

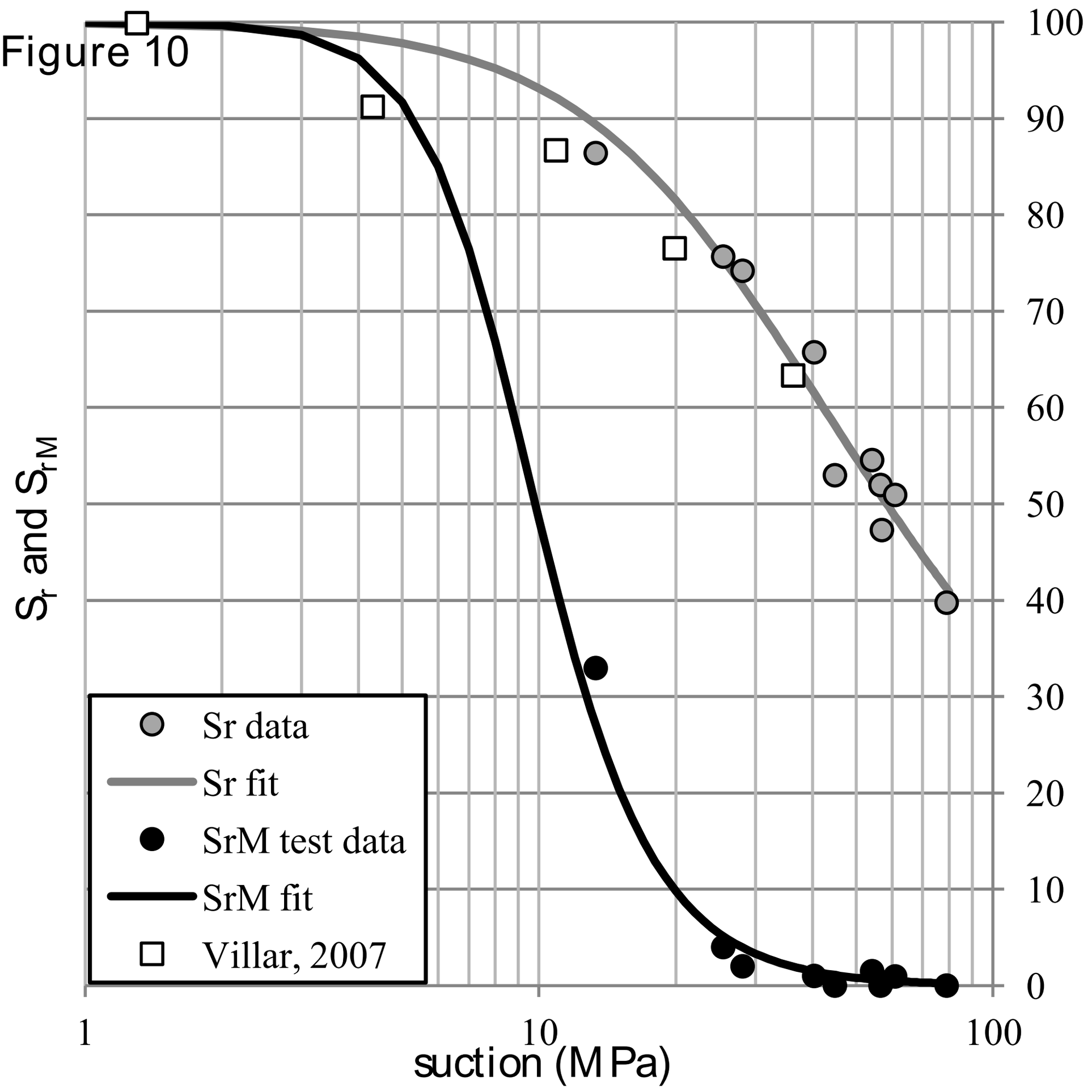
100
90
80
70
60
50
40
30
20
10
0
S_r and S_{rM}
Sr data
Sr fit
SrM test data
SrM fit
Villar, 2007
1
10
100
suction (MPa)

Figure 11

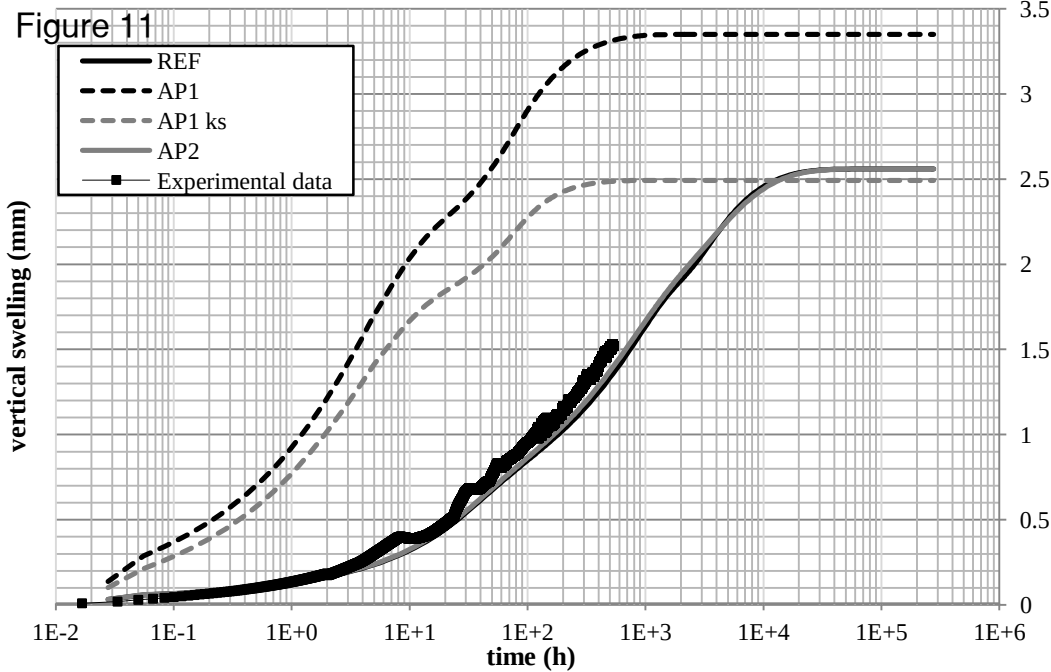
REF
AP1
AP1 ks
AP2
Experimental data
vertical swelling (mm)
time (h)
0
0.5
1
1.5
2
2.5
3
3.5
1E-2
1E-1
1E+0
1E+1
1E+2
1E+3
1E+4
1E+5
1E+6

Figure 12

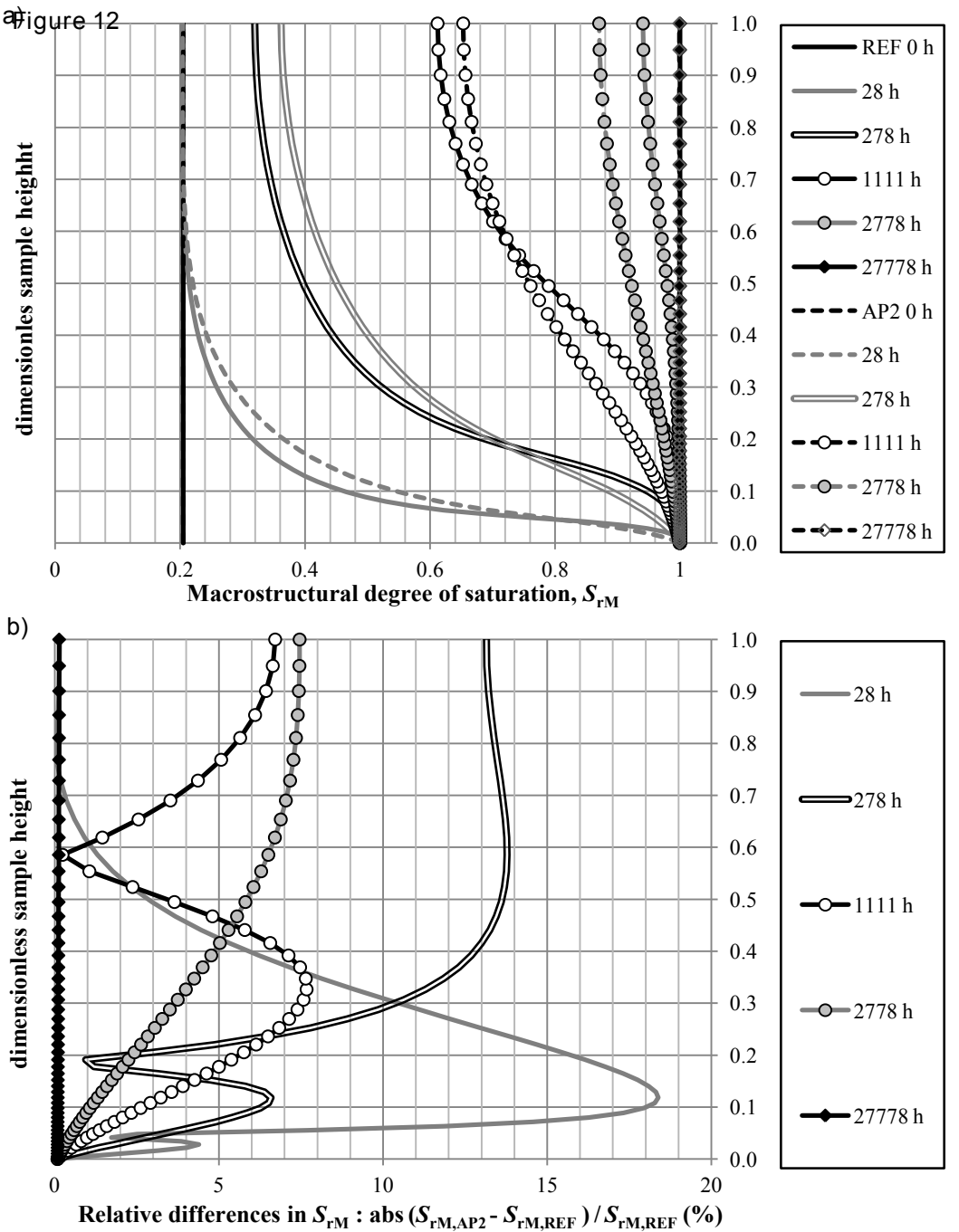
a)
dimensionles sample heighht
Macrostructural degree of saturation, S_{rM}
REF 0 h
28 h
278 h
1111 h
2778 h
27778 h
AP2 0 h
28 h
278 h
1111 h
2778 h
27778 h
b)
dimensionless sample height
Relative differences in S_{rM} : abs ($S_{rM,AP2}$ - $S_{rM,REF}$) / $S_{rM,REF}$ (%)
28 h
278 h
1111 h
2778 h
27778 h

Figure 13

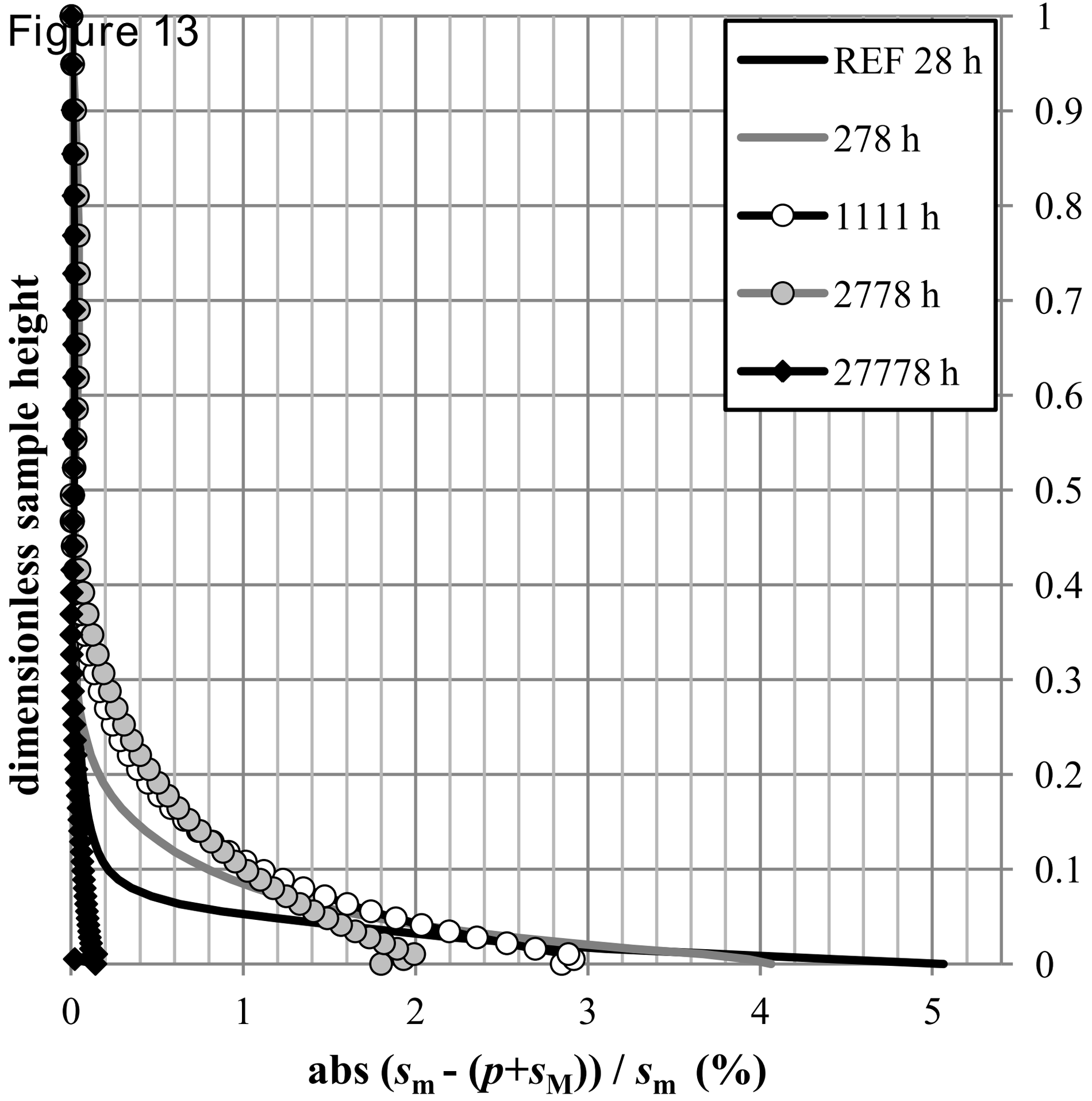
REF 28 h
278 h
1111 h
2778 h
27778 h
dimensionless sample height
0
0.1
0.2
0.3
0.4
0.5
0.6
0.7
0.8
0.9
1
0
1
2
3
4
5
abs (s_m - (p+s_M)) / s_m (%)

Figure 14

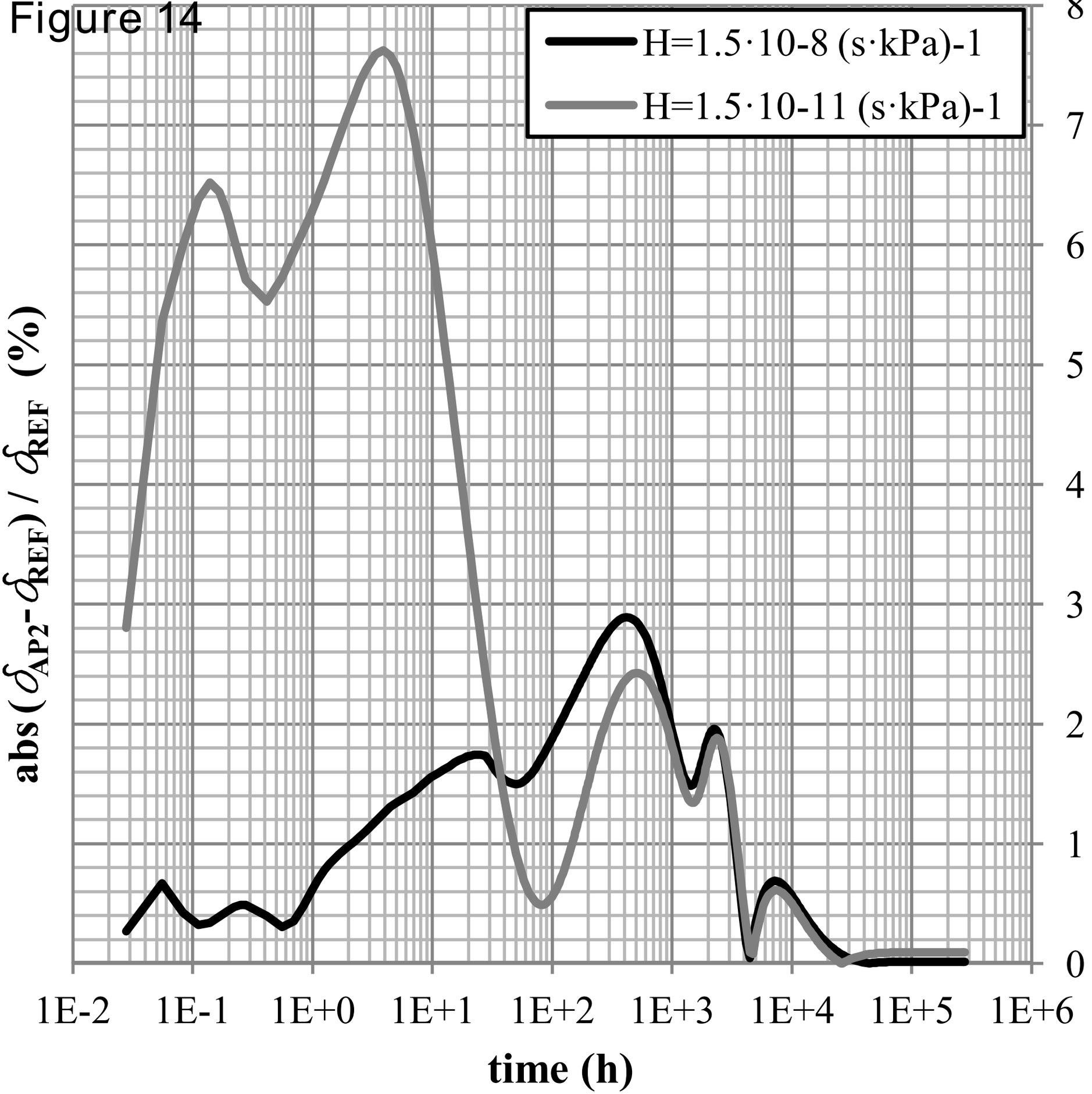
H=1.5·10-8 (s·kPa)-1
H=1.5·10-11 (s·kPa)-1
abs(δAP2-δREF) / δREF (%)
0
1
2
3
4
5
6
7
8
1E-2
1E-1
1E+0
1E+1
1E+2
1E+3
1E+4
1E+5
1E+6
time (h)

Fig. 1. Results obtained by B+Tech by applying the wetting paths described in Table 2 to the MX-80 characterised in Table 1.

Fig. 2. Results obtained by Dueck and Nilsson (2010) (SB_0_20 and 1_0_20 tests), Wadsö *et al*. (2004) and Kahr *et al*. (1990).

Fig. 3. Vertical swelling results of the isotropic swelling test performed at the University of Castilla-La Mancha.

Fig. 4. Retention curve (wetting path) of a Wyoming bentonite, adapted from Cases *et al*. (1992).

Fig. 5. Data associated with suctions greater than 40 MPa in Fig. 2 are used. (a) Relationship between the ratio $w_m \cdot (s_m^{1/3})$ and w_m. (b) Comparison between the experimental values of w_m and values of w_{mC} (obtained by using Eq. 2 and the variation of S presented by Salles *et al*., 2009). (c) Comparison between the experimental values of S obtained from Eq. 2 and the variation of S by Salles *et al*. (2009).

Fig. 6. Fit of e_{mC} values obtained with Eq. 15 to the experimental data from Fig. 2.

Fig. 7. Fit of the s_m-e_m values obtained with Eq. 16 to the experimental data from Fig. 2.

Fig. 8. Fit of the s_m-e_m values obtained with Eqs. 7, 8 and 15 to the experimental data from Fig. 2.

Fig. 9. Model (Eqs. 7, 8 and 16 and Table 4) and experimental s_m-e_m values from the tests of Fig. 1.

Fig. 10. Test and model values of S_r and S_{rM} from the tests shown in Fig. 1 (dry densities shown in Table 2 were used). Data from Villar (2007) are also included.

Fig. 11. Experimental (Fig. 3) and model vertical swelling results associated with different calculation approaches. The results from the REF and AP2 approaches overlap.

Fig. 12. (a) Comparison of the macrostructural degree of saturation values obtained with the REF and AP2 approaches. (b) Relative difference in the macrostructural degree of saturation values obtained with the REF and AP2 approaches.

Fig 13. REF approach: difference between s_m and $p+s_M$.

Fig 14. Evolution of the differences between the swelling strains obtained with the REF and AP2 approaches for different values of the transfer coefficient H.